

LAMOST observations in the *Kepler* field. Analysis of the stellar parameters measured with the LASP based on the low-resolution spectra*

Anbing Ren¹, Jianning Fu^{1,**}, Peter De Cat², Yue Wu³, Xiaohu Yang¹, Jianrong Shi³, Ali Luo³, Haotong Zhang³, Subo Dong⁴, Ruyuan Zhang¹, Yong Zhang⁵, Yonghui Hou⁵, Yuefei Wang⁵, Zihuang Cao³ and Bing Du³

Received 05-09-2016; accepted 06-27-2016

¹Department of Astronomy, Beijing Normal University, No. 19 Xijiekouwai Street, Haidian District, Beijing 100875, China, renanbing@gmail.com

²Royal observatory of Belgium, Ringlaan 3, B-1180 Brussel, Belgium

³Key Lab for Optical Astronomy, National Astronomical Observatories, Chinese Academy of Sciences, Beijing 100012, China

⁴Kavli Institute for Astronomy and Astrophysics, Peking University, Yi He Yuan Road 5, Hai Dian District, Beijing 100871, China

⁵Nanjing Institute of Astronomical Optics & Technology, National Astronomical Observatories, Chinese Academy of Sciences, Nanjing 210042, China

*Based on observations collected with the Large Sky Area Multi-Object Fiber Spectroscopic Telescope (LAMOST) located at the Xinglong Observatory, China.

**Send offprint request to: jnfu@bnu.edu.cn

ABSTRACT

All of the 14 subfields of the *Kepler* field have been observed at least once with the Large Sky Area Multi-Object Fiber Spectroscopic Telescope (LAMOST, Xinglong Observatory, China) during the 2012-2014 observation seasons. There are 88,628 reduced spectra with SNR_g (signal-to-noise ratio in g band) ≥ 6 after the first round (2012-2014) of observations for the LAMOST-*Kepler* project (LK-project). By adopting the upgraded version of the LAMOST Stellar Parameter pipeline (LASP), we have determined the atmospheric parameters (T_{eff} , $\log g$, and $[\text{Fe}/\text{H}]$) and heliocentric radial velocity v_{rad} for 51,406 stars with 61,226 spectra. Compared with atmospheric parameters derived from both high-resolution spectroscopy and asteroseismology method for common stars in [Huber et al. \(2014\)](#), an external calibration of LASP atmospheric parameters was made, leading to the determination of external errors for the giants and dwarfs, respectively. Multiple spectroscopic observations for the same objects of the LK-project were used to estimate the internal uncertainties of the atmospheric parameters as a function of SNR_g with the unbiased estimation method. The LASP atmospheric parameters were calibrated based on both the external and internal uncertainties for the giants and dwarfs, respectively. A general statistical analysis of the stellar parameters leads to discovery of 106 candidate metal-poor stars, 9 candidate very metal-poor stars, and 18 candidate high-velocity stars. Fitting formulae were obtained segmentally for both the calibrated atmospheric parameters of the LK-project and the KIC parameters with the common stars. The calibrated atmospheric parameters and radial velocities of the LK-project will be useful for studying stars in the *Kepler* field.

Subject headings: stars: general — stars: statistics — stars: fundamental parameters

— astronomical databases: miscellaneous

1. Introduction

The main scientific objective of the NASA (National Aeronautics and Space Administration) space mission *Kepler* are to detect the Earth-size and even larger planets in the habitable zone (Kasting et al. 1993; Borucki et al. 2007) of solar-like stars by using the method of photometric transits (Borucki et al. 2009), and to determine the properties of the planet host stars by means of asteroseismic methods (Christensen-Dalsgaard et al. 2007). Since the successful launch of *Kepler* on March 7, 2009, the number of stars having photometric time-series with an ultra-high precision of a few micro-magnitudes has increased steadily over a time-span of 4 years. As a large number of uninterrupted time-series has been obtained for pulsating stars of all kinds and flavors, the *Kepler* mission provides an unprecedented opportunity to study stellar oscillations. The *Kepler* Asteroseismic Science Consortium (KASC, Christensen-Dalsgaard et al. 2007), with a broad community participation, was established to select the most promising asteroseismic targets in the *Kepler* field of view (hereafter ‘*Kepler* field’) as targets for *Kepler* and to study their internal structure by means of asteroseismic methods (Gilliland et al. 2010; Chaplin et al. 2010). However, a reliable asteroseismic modeling requires reliable basic stellar physical parameters such as atmospheric parameters (the effective temperature T_{eff} , the surface gravity $\log g$, and the metallicity [Fe/H]) and the projected rotational velocity ($v \sin i$). Unfortunately, the atmospheric parameters as given in the *Kepler* Input Catalogue (KIC, Brown et al. 2011) are not always suited for a successful asteroseismic modeling as their errors amount to ~ 200 K in T_{eff} , and to ~ 0.5 dex in both $\log g$ and [Fe/H]. Moreover, KIC atmospheric parameters are missing for a significant fraction of the *Kepler* objects. The shortcomings of the stellar properties in the KIC have been quantified in follow-up studies and are summarized by Huber et al. (2014, hereafter H14).

During the last decade, a lot of ground-based observations have been gathered for a

wide variety of *Kepler* targets to support their space-based observations. An enormous observational effort involving 2-m class telescopes located in 12 countries in the northern hemisphere has been coordinated by [Uytterhoeven et al. \(2010a,b\)](#) for the observations of KASC objects, which leads to the characterization of, amongst others, OB-type stars (including candidate β Cephei and slowly pulsating B stars; [Catanzaro et al. 2010](#); [Lehmann et al. 2011](#); [Tkachenko et al. 2013](#)), AF-type stars (including candidate δ Scuti and γ Doradus stars; [Catanzaro et al. 2011](#); [Tkachenko et al. 2012, 2013](#); [Niemczura et al. 2015](#)), solar-like stars ([Molenda-Żakowicz et al. 2008](#); [Bruntt et al. 2012](#); [Karoff et al. 2013](#)), giants ([Bruntt et al. 2011](#)), and red giants ([Thygesen et al. 2012](#)). Though strong efforts have been made to characterize all types of asteroseismic targets, a significant fraction of the KASC targets remained unobserved, mainly because of the faintness of the targets and the unavailability of a sufficient amount of telescope time.

H14 presented an improved catalog for 196,468 stars observed by the NASA *Kepler* mission to support the study of the planet-occurrence rate by consolidating the published values of the atmospheric parameters (T_{eff} , $\log g$, $[\text{Fe}/\text{H}]$) that are derived with different observational techniques (mainly photometry, spectroscopy, asteroseismology and exoplanet transits). It is a valuable contribution to the improvement of the stellar properties of *Kepler* targets, but for a considerable fraction of stars, the KIC parameters could not be updated. Moreover, the consistency in the results is lacking as they are based on observations from heterogeneous devices and analysis techniques.

The LAMOST (the Large Sky Area Multi-Object Fiber Spectroscopic Telescope, also called the GuoShouJing Telescope) ([Su et al. 1998](#); [Zhao et al. 2012](#)), is a special 4-meter reflecting Schmidt telescope located at the Xinglong station of the National Astronomical Observatories of China ([Cui et al. 2012](#); [Luo et al. 2012](#)). Its focal length is 20 m and the focal plane, with a diameter of 1.75 m corresponding to a circular field of view of 5 degrees

on the sky (Wang et al. 1996), is covered with 4000 optical fibres connected to 16 two-arm low-resolution spectrographs with 32 CCD cameras. LAMOST spectra have a resolution of about 1800 and cover the wavelength range 370-900 nm (Cui et al. 2012; Zhao et al. 2012). The combination of a large aperture and a wide field of view covered by 4000 fibers makes LAMOST the most powerful optical spectroscopic survey instrument in the northern hemisphere at present. We therefore initiated the LAMOST-*Kepler* project (LK-project; De Cat et al. 2014) to acquire LAMOST spectra for as many objects in the *Kepler* field as possible and to characterize them in terms of spectral classification (spectral type with any peculiarities), atmospheric parameters (T_{eff} , $\log g$, $[\text{Fe}/\text{H}]$), rotation rate ($v \sin i$) and radial velocity (v_{rad}). It is the only way we can derive these parameters with an accuracy required for a detailed asteroseismic study for the vast majority of the *Kepler* objects in an efficient and homogeneous way. For a detailed description of the LK-project, we refer interested readers to De Cat et al. (2015).

The low-resolution LAMOST spectra available in the catalogue of the LK-project (De Cat et al. 2015) have been analysed by three different teams, each with their own independent method. This paper presents the analysis of the released parameters from the ‘Asian team’ (composed by the LAMOST project’s data processing department group and ABR, JNF, XHY group from Beijing Normal University) who determined the stellar atmospheric parameters by using the official LAMOST Stellar Parameter pipeline (LASP, Wu et al. 2014, 2011a; Luo et al. 2015). This paper is organized as follows. In Sections 2 and 3, brief descriptions of the observations and spectral data are given, respectively. A concise introduction of the LASP stellar parameter calculation is given in Section 4. In Section 5, LASP stellar parameters and their errors are calibrated based on the results from both external calibrations and internal uncertainties for the giants and dwarfs, respectively. Then we perform a statistical analysis of the calibrated atmospheric parameters and radial velocities present in the LASP catalogue in Section 6. It includes identifications of candidates

of particular objects. We compare calibrated LASP parameters with the values in KIC for common stars in Section 7. The paper is ended with conclusions and the prospect of the LK-project in Section 8.

2. Observations

2.1. Observation Plan

The *Kepler* field is relatively large (105 deg²). Fourteen circular LAMOST-*Kepler* fields (LK-fields) with a diameter of 5 degrees are needed for a close-to-full coverage of the *Kepler* field (see Figure 2 of De Cat et al. 2015). Some of these LK-fields are overlapped. To prepare the LAMOST observations of the 14 requested LK-fields, we constructed a prioritized target list which consists of targets from the KIC (*Kepler* targets’) supplemented with objects that have an absolute magnitude less than 20 in V band from the USNO-B catalogue (*field targets*’; Monet et al. 2003). We prioritized these objects within the *Kepler* field based on their coordinates (R.A. (2000) and Dec. (2000)), their brightness (the KIC magnitude K_p for most of the objects), the availability of their stellar parameters in the KIC (the effective temperature T_{eff} , the surface gravity $\log g$, and the metallicity [Fe/H]), and their scientific importance within the research community involved in the *Kepler* (see Section 2 of De Cat et al. 2015). For the first round of observations (2012-2014), from which the resulting LAMOST spectra are analysed in this paper, the top priority was assigned to the ~ 6500 targets that were of scientific interest for the *Kepler* Asteroseismic Science Consortium (KASC) at the beginning of the LK-project. Note that the *Kepler* field contains four open clusters, namely NGC6791, NGC6811, NGC6819 and NGC6866. Due to the density of the stars in the *Kepler* field, especially the regions containing the open clusters, it is impossible to observe all *Kepler* targets with LAMOST with only one round of observations. However, now that the observations of the *Kepler* mission have ended, the priority has shifted in the

next round of observation to the targets for which *Kepler* observations are available but for which no high-quality LAMOST spectrum is available yet. For more details about the construction of the target list, we refer the interested reader to Section 2 of [De Cat et al. \(2015\)](#).

2.2. Observation Progress

The observations for the LK-project started in May 2011, during the pilot survey period of LAMOST. As the observations started in the test phase of the LAMOST, the observations suffered from hardware and software failures in the beginning of the LK-project. Moreover, the *Kepler* field is best visible in the northern summer during which LAMOST is closed for several months due to the Monsoon. Therefore, some of the LK-fields had to be observed several times, and four observation seasons of the *Kepler* field were needed to complete the first round of observations (May 2011 - September 2014) in which all LK-fields were observed at least once under good conditions. Note that the spectra observed during the test phase of the LAMOST (before October 24, 2011) were omitted from the data products of the latest version (V2.7.5) of the data reduction and analysis pipeline because the telescope and instruments were still in the debugging stage at that time. The instability of the whole system led directly to the relatively low quality of the spectra. Although the catalogue of the LK-project contains a small proportion of spectra taken during the pilot survey with a sufficient quality, they are kept out of the catalogue of the LAMOST official data release. The updated LASP will not be applied to determine stellar parameters from the spectra that are observed before October 2011 and hence will not be included in the official data release of the LAMOST. So these spectra are omitted from our study too. In total, the 14 LK-fields were observed with 35 plates during 25 nights in the July 2012 - September 2014 observations seasons:

- 2012: 3 LK-fields with 7 plates during 3 nights,
- 2013: 6 LK-fields with 14 plates during 12 nights,
- 2014: 7 LK-fields with 14 plates during 10 nights.

For a detailed overview of the progress of the observations within the LK-project, we refer interested readers to Tables 1 & 2 and Section 5 of [De Cat et al. \(2015\)](#). In Table 1, we give an overview of the number of results obtained by the Asian team based on the LAMOST spectra gathered up to the end of the 2014 observation season of the *Kepler* field.

3. Spectral Data

3.1. Data Reduction

LAMOST has an automatic software system for its observation and data processing procedure (Luo et al. 2004; Wu et al. 2014). The goals of this system are to classify spectra and to calculate parameters from these spectra. The version V2.7.5 of the spectral reduction and analysis pipeline are used for the spectra obtained in the period 2012.06-2014.09. CCD Raw images from the LK-project were reduced and analyzed by the standard LAMOST automated data reduction and analysis system including the 2-dimension (2D) reduction pipeline (Luo et al. 2004), the 1-dimension (1D) pipeline, and the LAMOST stellar parameter pipeline - LASP (Wu et al. 2014; Luo et al. 2015). The CCD images are fed to the 2D reduction pipeline, which conforms with the spectral 2D pipeline of SDSS (Stoughton et al. 2002), to extract calibrated 1D spectrum in the format of FITS file for each object. The 2D pipeline includes seven basic tasks: dark and bias subtraction, flat field correction, spectra extraction, sky subtraction, wavelength calibration, sub-exposure merging and wavelength band combination. Simultaneously, the uncertainties in the wavelength and relative flux calibration are calculated in detail during this reduction process (Luo et al. 2015). The 1D pipeline, which is based on the specBS pipeline used for the analysis of SDSS spectra (Glazebrook et al. 1998), is to determine the spectral type of the stars and to automatically measure either the v_{rad} for stars or the redshift for galaxies and quasi-stellar objects (QSOs) by template matching and using a line recognition algorithm. The stellar templates were constructed by using accumulated LAMOST DR1 spectra (Wei et al. 2014). The main output of the spectral processing includes calibrated spectra with the corresponding analysis results and a catalog with information about the processed objects.

3.2. Data Release

The updated and calibrated spectra are provided to the astronomers at regular intervals. Up to September 2014, a total of 61,226 flux- and wavelength-calibrated, sky-subtracted low-resolution ($R=1800$) spectra and their LAMP stellar parameters were obtained during the first round of observations for the LK-project. These data will be released to the public along with the third data release (DR3¹) in June 2017. They can be downloaded from the official LAMOST website². The spatial distribution of the targets observed during the 2012-2014 observation seasons for the LK-project is shown in Figure 1. The database of low-resolution spectra of the LK-project consists of *Kepler* (61,218) and field targets (8) nearly covering the whole region of the *Kepler* field, except for one center and 4 off-center circle holes in each plate which contain the central bright star ($V < 8$; for the adaptive optics wave front sensor) and 4 guide stars ($V < 17$; for the guiding of the CCD cameras), respectively.

Figure 2 displays the histogram of the *Kepler* magnitude distribution of the dwarfs and giants in the LK-project. These targets are mainly distributed in the range of 11-15 *Kepler* magnitude (K_p) which indicates that only a small portion of bright and faint targets have been observed in the first observation round of the LK-project. The distribution of K_p also reflects the observation strategy of the LK-project under different conditions of observation. Indeed, the observations mainly focused on the very bright plates ($9 < r \leq 14$) in order to make full use of bright nights or nights with unfavourable weather conditions (e.g., poor seeing or low atmospheric transparency) (De Cat et al. 2015). Note that the K_p are not given in the KIC for 22 objects. Figure 3 shows the histograms of the signal-to-noise ratio (SNR) in the Sloan Digital Sky Survey (SDSS) u , g , r , i and z bands for the spectra in the

¹<http://dr3.lamost.org>

²www.lamost.org

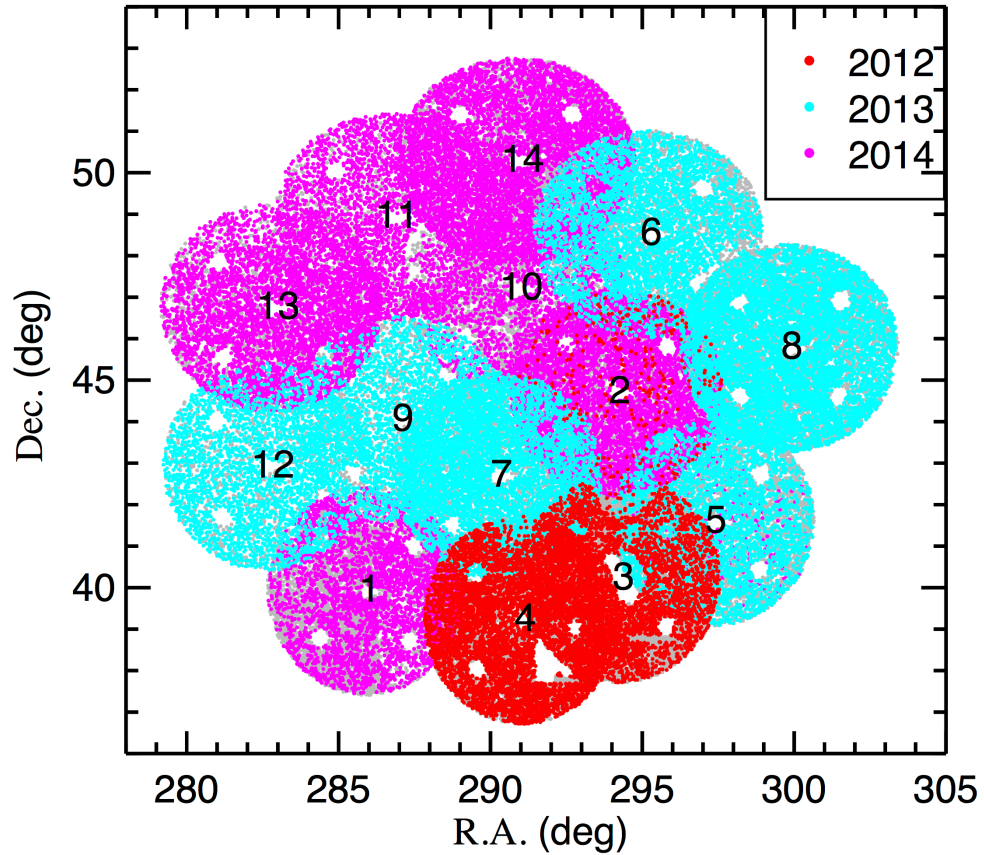


Fig. 1.— The spatial distribution of all the targets that were observed during the 2012-2014 observation seasons of the LK-project. The 51,406 targets for which we could derive the stellar parameters with LASP are given in colour (red for 2012; cyan for 2013; magenta for 2014) while all the others are given in grey.

catalog of data release, from top to bottom respectively. We take $\text{SNR}_g \geq 6$ and $\text{SNR}_g \geq 15$ as the criterion to retain the LAMOST spectra of the data release for stars that are observed during dark nights (eight nights before and after the new moon) and bright nights (all other nights except the three nights around the full moon in a lunar cycle), respectively (Luo et al. 2015). Hence, the distributions shown in the left panels of Figure 3 do not contain stars with $\text{SNR}_g < 6$ in the first bin (0-10).

Note that several problems have been found and fixed since the last DR2 update as described on the LAMOST data release website³. Based on the updated information of the wrong IDs of fiber, 9 fibers’ IDs of spectrograph 4 were found to be wrong since the survey in June 2012 for the observation of the LK-project. The regulation for calibrating the fibre position of spectrograph 4 is given in Table 2. It includes the fibre unit ID on the focal plane (Unitid) as given in the headers of the LAMOST 1D fits spectra, the old ID of the fibre (Fbid_old) and the corrected ID of the fibre (Fbid_now). Since the last three digits in the name of the LAMOST 1D fits file (Filename) represent the fibre’s ID, the wrong IDs of fibres lead to 71 Filenames in Table 4 of De Cat et al. (2015) are different from the Filenames in our Table . We adjusted the 71 Filenames following the rules of calibration for the fibre position in order to obtain the KIC IDs for observed targets from the Table 4 by matching the Filenames. The revised Filenames are indicated with a letter ‘c’ after the name of the fits file in the ‘Filename’ column of Table 3.

4. Stellar Parameter Calculation

An upgraded version of the LASP was used to automatically determine the stellar atmospheric parameters (T_{eff} , $\log g$ and $[\text{Fe}/\text{H}]$) and radial velocity (v_{rad}) from fits spectra

³<http://dr2.lamost.org>

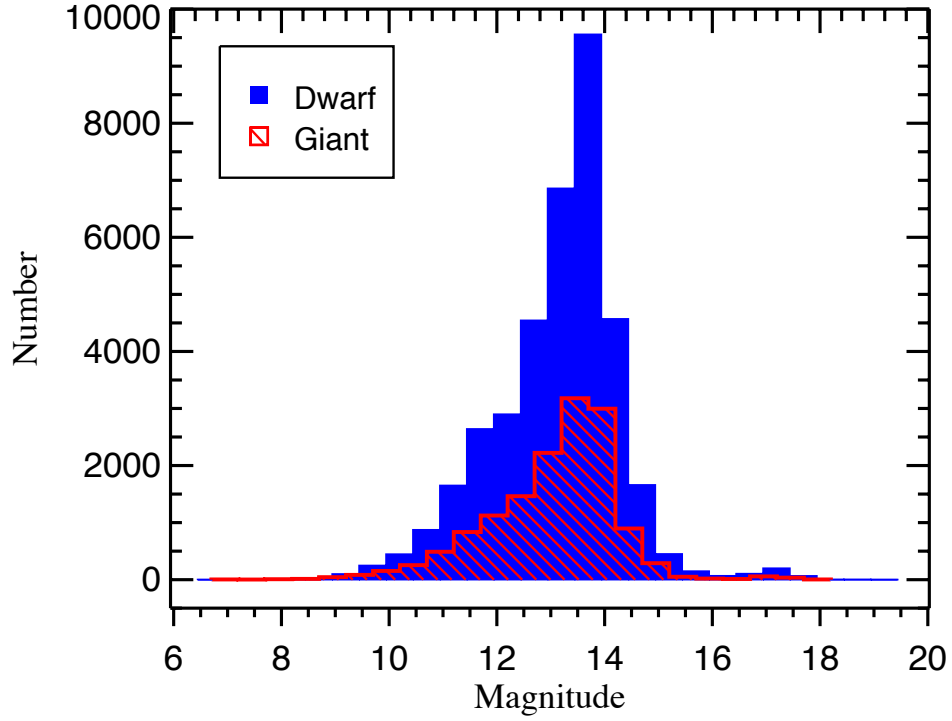


Fig. 2.— The distribution of the *Kepler* magnitude (K_p) as given in the KIC for the dwarfs (blue) and giants (red), respectively.

Table 2. The regulation for calibrating the fibre position of spectrograph 4.

Unitid	Fbid_old	Fbid_now
F3229	76	87
F3230	87	79
F3231	79	95
F3232	95	84
F3333	84	76
H3129	44	31
H3130	31	46
H3131	46	26
H3132	26	44

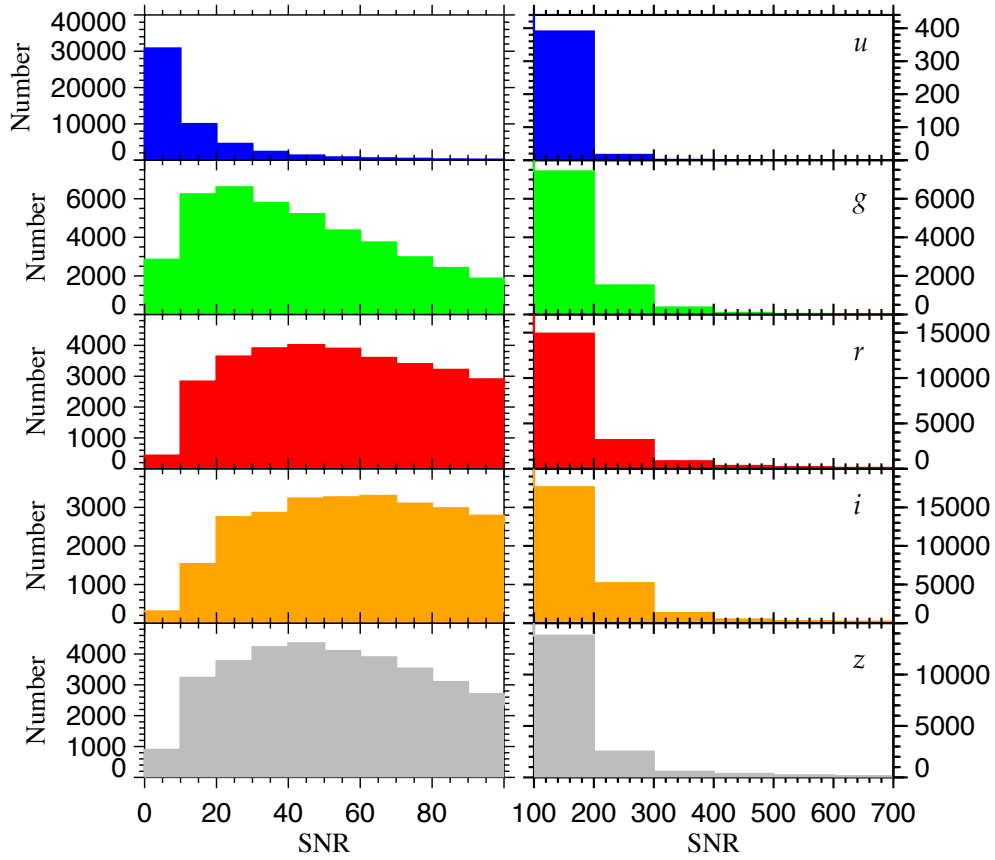


Fig. 3.— The distribution of the signal-to-noise ratio in the SDSS u , g , r , i and z bands, given from top to bottom respectively. The left and right panels show the SNR range from 0 to 100 with binsize 10 and the SNR range from 100 to 700 with binsize 100, respectively.

products of the 2D and 1D pipelines in the spectral database of the LK-project. The SNR_g of these spectra are greater than or equal to 6 and 15 for the dark nights and bright nights, respectively. We select the spectra with STAR as *final_class* and late A, F, G or K as *final_subclass* to determine their stellar parameters. Both the CFI (Correlation Function Initial) and ULYSS (Université de Lyon Spectroscopic analysis Software; Wu et al. 2011b) methods are consecutively applied to determine the stellar parameters in the processing procedure of LASP. More information about the progress of stellar parameters calculation is given by Luo et al. (2015).

We determined the stellar atmospheric parameters (T_{eff} , $\log g$ [Fe/H]), radial velocity (v_{rad}) and their errors for the selected 61,226 ($\sim 60.6\%$) of the 101,086 low-resolution LAMOST spectra available in the catalogue of the LK-project after completion of the first round of observations (De Cat et al. 2015). As some of the LK-fields have been observed more than once and there are some overlaps between some of the fields, a fraction of the observed stars have multiple LAMOST observations. Hence, the 61,226 analysed LAMOST spectra correspond to 51,406 unique targets, including 671 A-type stars, 18,937 F-type stars, 25,847 G-type stars, and 5,952 K-type stars. These targets are indicated in colour on Figure 1: red for 2012, cyan for 2013, and magenta for 2014. Apart from the central and off-center holes typical for each plate, it is clear that there are still several other block-like regions for which we could not determine the stellar parameters from the available LAMOST spectra (given in grey). This is a reflection of problems with some spectrographs in these parts.

In Table 3, we give the information about these targets including the following columns:

1. column 1: The unique spectra ID (Obsid).
2. column 2: The file name of the LAMOST 1D fits file (Filename).

3. column 3: The final identification of the target after cross-identification with the Table 4 of [De Cat et al. \(2015\)](#) by the Filename (Target).
4. column 4: The observed right ascension in degrees (R.A.).
5. column 5: The observed declination in degrees (Dec.).
6. column 6: The magnitude in the KIC for this target (K_p).
7. column 7: The date and time of observation (yyyy-mm-ddThh:mm:ss.ss).
8. column 8: The spectral sub-class retrieved from the 1D fits files (Subclass).
9. column 9: The value of SNR in the g -band (SNR_g).
10. column 10: the effective temperature (T_{eff}) in K and its error giving by the LASP.
11. column 11: The surface gravity ($\log g$) in dex and its error giving by the LASP.
12. column 12: The metallicity ($[\text{Fe}/\text{H}]$) in dex and its error giving by the LASP.
13. column 13: The radial velocity (v_{rad}) in km s^{-1} and its error giving by the LASP.
14. column 14: The information whether the object has been observed by the *Kepler* mission (KO).

Table 3. The catalogue of the LASP stellar parameters for the LK-project.

Obsid	Filename	Target	R.A. (deg)	Dec. (deg)	K_p	yyyy-mm-ddThh:mm:ss.ss
Subclass	SNR _g	T_{eff} (K)	$\log g$ (dex)	[Fe/H] (dex)	v_{rad} (km s^{-1})	KO
52201011	spec-56083-IF04_B56083_sp01-011	KIC07042868	294.51886	42.549595	9.117	2012-06-04T18:35:33.32
G5	76.73	4852.00±51.72	2.658±0.470	-0.021±0.082	1.98±12.52	N
52201018	spec-56083-IF04_B56083_sp01-018	KIC06957157	294.34372	42.407665	10.106	2012-06-04T18:35:33.32
G5	50.72	4742.09±64.08	2.497±0.455	-0.002±0.098	6.07±11.74	Y
...
24310476	spec-56811-KP190339N395439V02_sp04-076c	KIC04347646	285.90503	39.466915	12.552	2014-06-02T18:57:40.48
F9	55.97	4941.71±126.43	2.355±0.768	-0.694±0.208	-14.05±19.06	Y
24310477	spec-56811-KP190339N395439V02_sp04-077	KIC04244973	286.03354	39.327650	10.305	2014-06-02T18:57:40.48
G5	20.67	4811.94±142.05	2.872±0.533	-0.010±0.189	-20.98±13.93	Y
...
250013110	spec-56930-KP192323N501616V03_sp13-110	1350-10735728	293.58322	51.240780		2014-09-29T12:29:21.91
F6	16.53	6058.80±93.06	4.220±0.302	-0.142±0.140	-9.03±16.17	N
250013119	spec-56930-KP192323N501616V03_sp13-119	KIC12361114	293.69366	51.197147	11.178	2014-09-29T12:29:21.91
F0	86.22	6708.83±51.12	3.536±0.265	-0.012±0.088	-35.16±17.78	N
...
250016248	spec-56930-KP192323N501616V03_sp16-248	KIC12933571	289.32538	52.398720	13.307	2014-09-29T12:29:22.02
K5	19.47	4480.25±49.50	2.678±0.333	-0.266±0.077	-89.24±8.66	N
250016249	spec-56930-KP192323N501616V03_sp16-249	KIC12883443	289.20694	52.250880	13.460	2014-09-29T12:29:22.02
K0	18.22	5286.27±102.40	3.808±0.468	0.035±0.138	-49.52±13.55	N

The unique spectra ID (Obsid) is in the first column, the name of the LAMOST 1D fits file (Filename) is in column 2, the KIC ID for these targets (Target) is in column 3, the columns from 4 to 8 are for the information extracted from the headers of the LAMOST 1D fits files: the observed right ascension (R.A.) and declination (Dec.) in degrees, the magnitude in the KIC (K_p), the mid-time of observation (yyyy-mm-ddThh:mm:ss.ss), the sub-classification for targets (Subclass), the value of SNR_g. The next four columns give the LASP stellar parameters (T_{eff} , $\log g$, [Fe/H] and v_{rad}) and their uncertainties. The last column gives the information whether the object has been observed by the *Kepler* mission (KO, Y=YES, N=NO).

5. Calibration of Stellar Parameters

The stellar atmospheric parameters of the LK-project targets that are listed in Table 3 are compared with the common targets in a sub-sample of H14 to perform an external calibration of LASP atmospheric parameter uncertainties for the giants and dwarfs, respectively. On the other hand, multiple observation targets in the parameter catalogue of the LK-project are used to obtain the internal calibration of these parameter uncertainties. Then we recalibrate the LASP stellar parameters based on the results of external calibration and internal calibration for the giants and dwarfs, respectively.

5.1. External Calibration

For the external calibration of the LASP results, we used the atmospheric parameters for stars in the *Kepler* field based on *Spectroscopy* and *Asteroseismology* as given by H14 (categories C1, C2, C3, C7, C8, and C9 of their Table 1) as the most reliable reference. Given the large dispersion in the methods used for the parameter determination of the literature values originating from [Uytterhoeven et al. \(2011\)](#) (indicated with ‘SPE4’ in H14), these values were excluded. The remaining sample of stars was cross-identified with those listed in Table 3 to determining the common stars. Based on the choice of the classification for the dwarfs and giants in H14, these common stars were divided into giant stars ($\log g < 3.5$) and dwarf stars ($\log g \geq 3.5$) to verify the reliability of the LASP parameters of both groups individually. For all the stars in this common subset, we select the T_{eff} and $[\text{Fe}/\text{H}]$ values given by H14 that were derived from high-resolution ($R \geq 20,000$) spectroscopic data with analysis pipelines such as SME (Spectroscopy Made Easy; [Valenti & Piskunov 1996](#)), SPC (Stellar Parameter Classification; [Buchhave et al. 2012](#)), VWA (Versatile Wavelength Analysis; [Bruntt et al. 2010](#)), and ROTFIT ([Frasca et al. 2003](#)). The values of $\log g$ were obtained from asteroseismology and spectroscopy. The comparison of atmospheric

parameters for the giants and dwarfs in common between the select sub-sample of H14 and the catalogue of the LK-project is presented in Figure 4.

Figure 4(a) shows the comparison of T_{eff} for giant stars. The full line in the upper panel gives the result of a linear fit to the data:

$$T_{\text{eff,LASP}} = (0.94 \pm 0.02)T_{\text{eff,Huber}} + (299 \pm 104) \text{ (for giants) ,} \quad (1)$$

where the subscript ‘LASP’ indicates the parameters that are derived by LASP from LAMOST spectra while the subscript ‘Huber’ means that the parameters originate from Table 4 of Huber et al. (2014, hereafter HT4). The slope slightly smaller than unit, the best fit indicates that the $T_{\text{eff,LASP}}$ values are slightly higher than those given by H14 at the low temperature region while it is the other way around at the high temperature region. The values derived from the LAMOST low-resolution spectra correlate well with those obtained from the high-resolution spectra in the T_{eff} range of 3,800 K to 5,300 K. The mean difference and the standard deviation σT_{eff} of the residuals ($\Delta T_{\text{eff}} = T_{\text{eff,LASP}} - T_{\text{eff,Huber}}$) amount to 34 K and 131 K, respectively. Only one targets KIC11559263, classified by LASP as a G1 star with the effective temperature 5780 ± 66 K, is located outside the 3σ region around the mean difference. We checked this LAMOST spectrum and found that it’s quality is very good: the SNR_g reaches 150 and the error of T_{eff} is smaller than the one given in the literature. In general, the errors of T_{eff} from the LASP results are smaller than the typical adopted uncertainties as given by H14. The comparison of the T_{eff} values for dwarf stars is shown in Figure 4(d). Compared to the result of the giant stars, a tighter relation is found between the T_{eff} values for the dwarf stars:

$$T_{\text{eff,LASP}} = (1.02 \pm 0.02)T_{\text{eff,Huber}} + (99 \pm 93) \text{ (for dwarfs)} \quad (2)$$

in the T_{eff} range of 3,900 K to 7,000 K, although 4 stars (green points) deviate from the 3 times σ region around the mean difference. These stars are KIC04832837, KIC12644769,

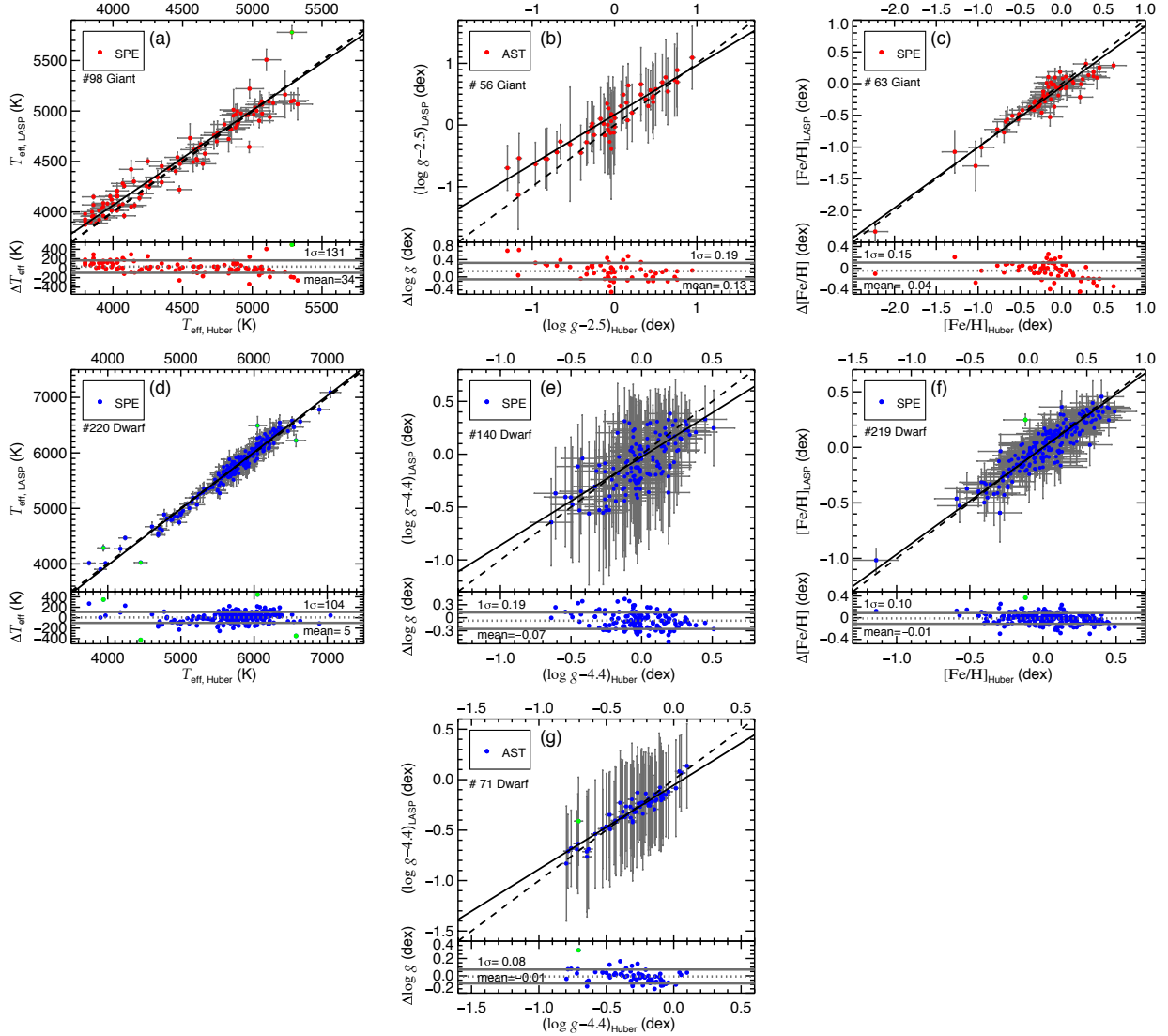


Fig. 4.— Comparison of the T_{eff} , $\log g$ and $[\text{Fe}/\text{H}]$ as determined by LASP (LASP, Y-axis of the upper panels) with the subset for which the stellar parameters were derived by the method of spectroscopy (SPE) and asteroseismology (AST) in HT4 (categories C1, C2, C3, C7, C8, and C9 of their Table 1; X-axis). The parameters derived from high resolution spectra are mainly based on 8 works (Batalha et al. 2013; Bruntt et al. 2012; Buchhave et al. 2012; Huber et al. 2013; Mann et al. 2012; Molenda-Żakowicz et al. 2013; Petigura et al. 2013; Thygesen et al. 2012). In the upper panels, the stars in common between the two data sets are plotted with their error bars. The black dashed line visualises the bisector while the black solid line is a linear fit to the datapoints. In the lower panels, the difference (LASP - Huber) for these parameters are plotted on Y-axis. The mean bias is indicated by the dotted line and the grey solid line is the 1σ deviation. The results for the giants and dwarfs are given in red and blue, respectively. The stars for which the values are found outside the 3σ region around the mean difference are given in green.

KIC12454461 and KIC08346342 from low to high temperature, respectively. KIC04832837 and KIC12644769 are classified as K5 and K7 type stars with a temperature of 4288 ± 56 K and 4024 ± 21 K, respectively. Their spectra have a good quality with $\text{SNR}_g=15$ and 64, respectively. A problem with the background subtraction results in negative fluxes and a wrong combination of the blue and red channel for the LAMOST spectrum of KIC12454461. Hence, the LASP T_{eff} derived from this spectrum, even if it has a high SNR ($\text{SNR}_g=77$), is unreliable. The LASP value of KIC08346342 (a F6 type star with $T_{\text{eff}}=6224 \pm 111$ K) is more trustworthy given the high quality of its LAMOST spectrum and its error below the uncertainties given by H14.

The comparison of the $\log g$ values that are calculated by the asteroseismic method for giant stars is given in Figure 4(b). The linear relation of the $\log g$ between the LASP and Huber is described by the following function:

$$(\log g - 2.5)_{\text{LASP}} = (0.80 \pm 0.12)(\log g - 2.5)_{\text{Huber}} + (0.17 \pm 0.06) \text{ (for giants)}. \quad (3)$$

The mean difference and standard deviation $\sigma \log g$ of the residuals ($\Delta \log g = \log g_{\text{LASP}} - \log g_{\text{Huber}}$) amount to 0.13 dex and 0.19 dex, respectively. The $\log g_{\text{LASP}}$ values tend to be slightly higher than the published values, especially in the range of $(\log g - 2.5)_{\text{Huber}} < 0.5$ dex for most giant stars. Liu et al. (2014) estimated the surface gravity of LAMOST giant stars by using the support vector regression model based on the *Kepler* measured seismic surface gravities given by H14. They also revealed a systematic overestimation of $\log g_{\text{LASP}}$ for some giant stars ($\log g < 4.0$ dex and $[\text{Fe}/\text{H}] > -0.6$ dex). The comparisons of the $\log g$ derived from spectroscopy (SPE) and asteroseismology (AST) for the dwarfs are shown in Figure 4(e) and (g), respectively. The data are fitted slightly better by a global linear relation than Figure 4(b) (full black line). We obtained the following linear fit as the best approximation for the relation of the $\log g$ values for the 211 common dwarf stars:

$$(\log g - 4.4)_{\text{LASP}} = (0.86 \pm 0.11)(\log g - 4.4)_{\text{Huber}} - (0.03 \pm 0.03) \text{ (for dwarfs)}. \quad (4)$$

We still can find the overestimation of $\log g$ for the dwarf stars with $(\log g - 4.4)_{\text{Huber}} < -0.4$ dex. Although LAMP slightly underestimates the overall $\log g$ values for the dwarf stars, there is an overestimation trend towards decreasing $\log g$ values. Note that the errors of LAMOST surface gravities are almost always larger than the uncertainties given by H14 because of the high-precision of $\log g$ derived with the method of asteroseismology (Morel & Miglio 2012; Creevey et al. 2013; Epstein 2015) and from high-resolution spectra. The mean difference and standard deviation of $\Delta \log g$ are -0.07 ± 0.19 dex and -0.01 ± 0.08 dex for dwarf stars as compared to the values derived from high-resolution spectra and by the method of asteroseismology, respectively. For all dwarf stars, the mean difference and standard deviation of $\Delta \log g$ is -0.05 ± 0.16 dex. The F5 star KIC07800289 ($\log g = 3.99 \pm 0.44$ dex) is located out the 3σ region around the mean difference even though its LAMOST spectrum is of excellent quality ($\text{SNR}_g = 156.9$). It is shown as green point in Figure 4(g).

The linear correlations

$$[\text{Fe}/\text{H}]_{\text{LASP}} = (0.95 \pm 0.06)[\text{Fe}/\text{H}]_{\text{Huber}} - (0.05 \pm 0.03) \text{ (for giants) and} \quad (5)$$

$$[\text{Fe}/\text{H}]_{\text{LASP}} = (0.96 \pm 0.06)[\text{Fe}/\text{H}]_{\text{Huber}} - (0.00 \pm 0.01) \text{ (for dwarfs) ,} \quad (6)$$

which are close to the 1:1 relation, are found as the best fit for the relation between the $[\text{Fe}/\text{H}]$ values for the common giant and dwarf stars and are plotted as a black full line in Figure 4(c) and (f), respectively. The majority of the residual $[\text{Fe}/\text{H}]$ values ($\Delta[\text{Fe}/\text{H}] = [\text{Fe}/\text{H}]_{\text{LASP}} - [\text{Fe}/\text{H}]_{\text{Huber}}$) are concentrated around 0 dex. Only a small fraction of them are found outside the 3σ $\Delta[\text{Fe}/\text{H}]$ region. The reliability of the $[\text{Fe}/\text{H}]$ derived from the LAMOST low-resolution spectra with the LAMP have already received recognition by comparison with results derived from the high-resolution spectra in a relatively small metallicity range of -0.3 dex to +0.4 dex (Dong et al. 2014). Our comparison shows that the $[\text{Fe}/\text{H}]$ values obtained with LAMP are reliable in the range between -1.0 dex and 0.5 dex for giant stars, and between -0.6 dex and 0.5 dex for dwarf stars. We note that

LASP underestimates $[\text{Fe}/\text{H}]$ for the giant stars in the range $[\text{Fe}/\text{H}] > 0.2$ dex. The mean differences and standard deviations of $\Delta[\text{Fe}/\text{H}]$ are -0.04 ± 0.15 dex and -0.01 ± 0.10 dex for giant and dwarf stars, respectively. The discrepant object, the value of $\Delta[\text{Fe}/\text{H}]$ deviate from the 3σ region around the mean difference, shown as a green point in Figure 4(f) is KIC10318874 ($[\text{Fe}/\text{H}] = 0.25 \pm 0.05$ dex, $\text{SNR}_g = 85$). It has been classified by LASP as a F5 dwarf star. The LAMOST spectrum of this star is of good quality and the error on the metallicity is relatively low, which are both in favour to consider the LASP results as trustworthy.

Comparisons between the LASP parameters and those listed in the considered sub-sample of HT4 illustrate that the correlation of these parameters is close to the 1:1 relation. This result favors the reliability of the LASP determinations in wide ranges: from 3,800 K to 6,600 K for T_{eff} , from 1.5 dex and 4.9 dex for $\log g$ and from -1.0 dex to 0.5 dex for $[\text{Fe}/\text{H}]$. Note that the reliable ranges of atmosphere parameters are not completely the same for giant and dwarf stars. We need more stars with values outside those ranges to validate the reliability of the LASP results. The atmospheric parameters of the dwarfs in the LK-project are superior to the values of the giants in general as shown in the Figure 4.

5.2. Internal Calibration

In total, 7 LK-fields have been observed more than once from 2012 to 2014 as given in the upper part of Table 1. Moreover, there is overlap between adjacent LK-fields to allow a full coverage of the *Kepler* field as shown in Figure 1. Hence, we obtained more than one spectrum for a substantial fraction of stars: 7,550 stars have been observed two times, 986 stars three times, 92 stars four times, and 5 stars at least five times (bottom part of Table 1). The atmospheric parameters of these stars have been derived from the spectra of multiple observations.

We assess the internal errors of stellar atmospheric parameters by making comparisons of the atmospheric parameters obtained from different LAMOST spectra of the same objects. We used the method of the unbiased estimator:

$$\Delta P_i = \sqrt{n/(n-1)}(P_i - \bar{P}), \quad (7)$$

with $i = 1, 2, \dots, n$, where i is one of the individual measurements and n is the total number of measurements for parameter P (Xie et al. 2016). The values of the unbiased estimations for the effective temperature (ΔT_{eff}), surface gravity ($\Delta \log g$) and metallicity ($\Delta[\text{Fe}/\text{H}]$) versus SNR_g of the LAMOST spectra are shown in Figure 5, respectively. Second-order polynomials as a function of SNR_g are used to fit the 1σ confidence interval in various bins of SNR_g . The following fitting functions are given as red solid lines:

$$\begin{cases} \sigma_{T_{\text{eff}}} = 47.0X^2 - 232.1X + 342.1 \text{ K} \\ \sigma_{\log g} = 0.070X^2 - 0.366X + 0.532 \text{ dex} \\ \sigma_{[\text{Fe}/\text{H}]} = 0.045X^2 - 0.253X + 0.386 \text{ dex} \end{cases} \quad (8)$$

where X is the base-10 logarithm of SNR_g . The internal errors of the parameters with the $\text{SNR}_g \geq 6.0$ are 91 K, 0.12 dex and 0.09 dex for T_{eff} , $\log g$ and $[\text{Fe}/\text{H}]$, respectively. For the stars with $\text{SNR}_g \geq 50$, the inner errors of them are 68 K, 0.08 dex and 0.06 dex, respectively.

5.3. Calibration of LASP Stellar Parameters

The external calibration of the LASP stellar parameter uncertainties for giants and dwarfs are obtained by a separate comparison with the published values in HT4 as described in Section 5.1. The internal errors of the stellar atmospheric parameters as a function of the base-10 logarithm of SNR_g are calculated using the parameters of multiple observations objects as described in Section 5.2. The dispersions of the LASP stellar atmospheric

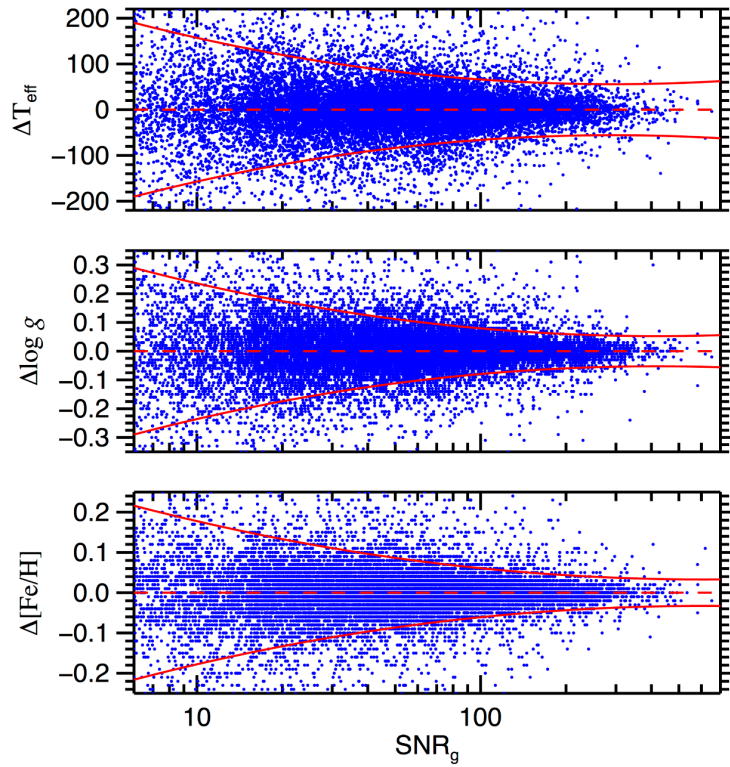


Fig. 5.— The unbiased estimation for the multiple observation targets as a function of SNR_g (blue dots). The 1σ confidence levels are fitted with a second-order polynomial (red solid lines).

parameter uncertainties (the green lines), taking both intern and external uncertainties into account, are calculated for the giants (left panels) and dwarfs (right panels) in Figure 6, respectively. The relation between the differences (LASP - Huber) and SNR_g are shown for the common giants (red points) and dwarfs (blue points) when compared with the published values in HT4 as described in Figure 4. The black dashed lines describe the mean biases of the parameters.

The external and internal uncertainties of the LASP parameters are combined to redefine the systematic deviation and the errors of stellar atmospheric parameters within the LK-project. The calibrated relations are given by:

$$\begin{cases} P_i = (P_{i,\text{LASP}} - a)/b \\ \sigma = \sqrt{\sigma_{in}^2 + \sigma_{ex}^2} \end{cases} \quad (9)$$

where for each observation i , P_i denotes the calibrated stellar parameters and $P_{i,\text{LASP}}$ is the LASP value while a and b are the zero and slope of the linear functions as given in Section 5.1. σ is the calibrated errors of atmospheric parameters. σ_{in} is the inner deviation described by a second-order polynomial as a function of SNR_g by fitting the data points of the unbiased estimation for targets with multiple observations (see Section 5.2 & Figure 5). σ_{ex} is the external deviation of the LASP atmospheric parameter uncertainties (see Section 5.1). Based on these calibrated relations, we recalculated the LASP stellar parameters according to the following formulae for giant and dwarf stars, respectively:

$$T_{\text{eff}} \begin{cases} \sigma_{in} = 47.0X^2 - 232.1X + 342.1 \text{ K} \\ a = 299 \text{ K}, b = 0.94; \sigma_{ex} = 131 \text{ K (for giants)} \\ a = 99 \text{ K}, b = 1.02; \sigma_{ex} = 104 \text{ K (for dwarfs)}, \end{cases} \quad (10)$$

$$\log g \begin{cases} \sigma_{in} = 0.070X^2 - 0.366X + 0.532 \text{ dex} \\ a = 0.67 \text{ dex}, b = 0.80; \sigma_{ex} = 0.19 \text{ dex (for giants)} \\ a = 0.59 \text{ dex}, b = 0.86; \sigma_{ex} = 0.16 \text{ dex (for dwarfs)}, \end{cases} \quad (11)$$

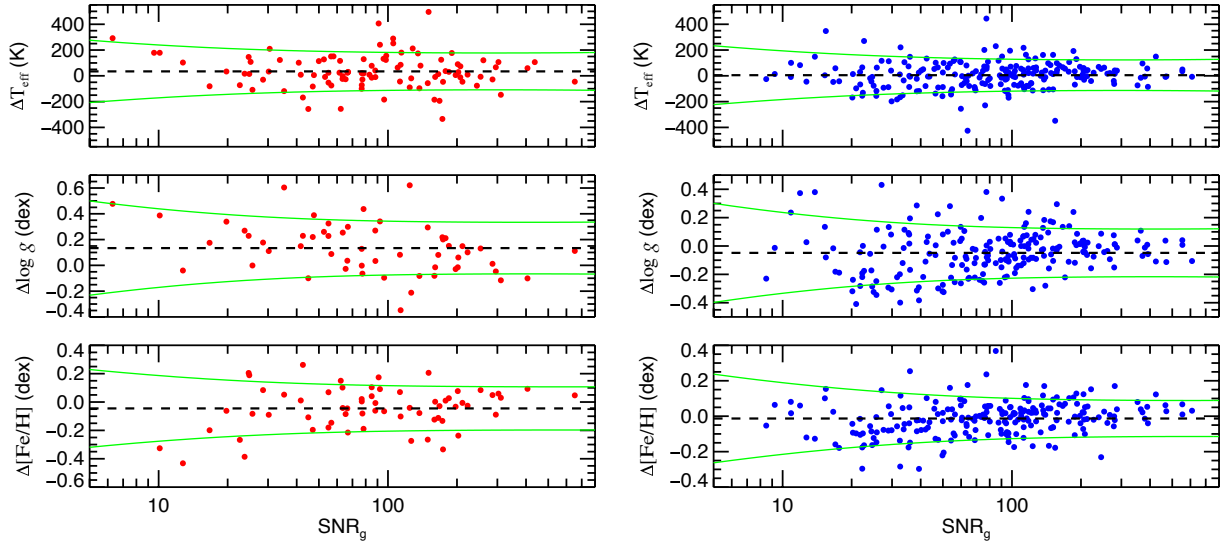


Fig. 6.— The dispersions of the LASP stellar atmospheric parameter uncertainties (the green lines), taking both intern and external uncertainties into account, are calculated for the giants (left panels) and dwarfs (right panels), respectively. The mean biases are indicated by the black dashed lines when compared with the published values in HT4, the red points and blue points represent the relation between the differences (LASP - Huber) and SNR_g for the common giants and dwarfs, respectively.

$$[\text{FeH}] \begin{cases} \sigma_{in} = 0.045X^2 - 0.253X + 0.386 \text{ dex} \\ a = 0.05 \text{ dex}, b = 0.95; \sigma_{ex} = 0.15 \text{ dex (for giants)} \\ a = 0.00 \text{ dex}, b = 0.96; \sigma_{ex} = 0.10 \text{ dex (for dwarfs)}, \end{cases} \quad (12)$$

where X is the base-10 logarithm of SNR_g . The calibrated atmospheric parameters and their errors are listed in Table 4, which includes ‘Obsid’, ‘Target’ and the information of the spectra as listed in Table 3.

6. Statistical Analysis of Stellar Parameters

For 8,633 targets, more than one spectrum of LAMOST observation have been analyzed (see bottom rows of Table 1). We determined the stellar parameters from the multiple LAMOST spectra with different SNR values. The accuracy and credibility of these parameters mainly depends on the quality of the observed spectra. For these stars with multiple observations, we refer to the parameters that are derived from the LAMOST spectrum with the highest SNR_g in what follows (unless stated otherwise). We provide a general statistical analysis of stellar parameters for all 51,399 *Kepler* stars in the LK-project.

The calibrated LAMP stellar atmospheric parameters (T_{eff} , $\log g$ and $[\text{Fe}/\text{H}]$) and the LAMP v_{rad} are found in the ranges 3,678 \sim 8,275 K, -1.150 \sim 6.174 dex, -2.811 \sim 1.105 dex and -472 \sim 120 km/s, respectively. The mean errors of the measured stellar parameters are 2.75% in T_{eff} , 0.215 dex in $\log g$, 0.152 dex in $[\text{Fe}/\text{H}]$, and 18 km s $^{-1}$ in v_{rad} . In Figure 7, the analyzed stars are plotted in the $T_{\text{eff}} - \log g$ diagram (so-called ‘Kiel’ diagram). As can be seen, they are mainly located in the main sequence and the classical instability strip.

Figure 8 shows the histograms of T_{eff} , $\log g$, $[\text{Fe}/\text{H}]$ and v_{rad} , which helps to easily find the stars of particular interest in the LK-project, such as metal-poor stars (Li et al. 2015a,b; Aoki 2014; Wu et al. 2010) and high velocity stars (Zhong et al. 2014). Two distinct

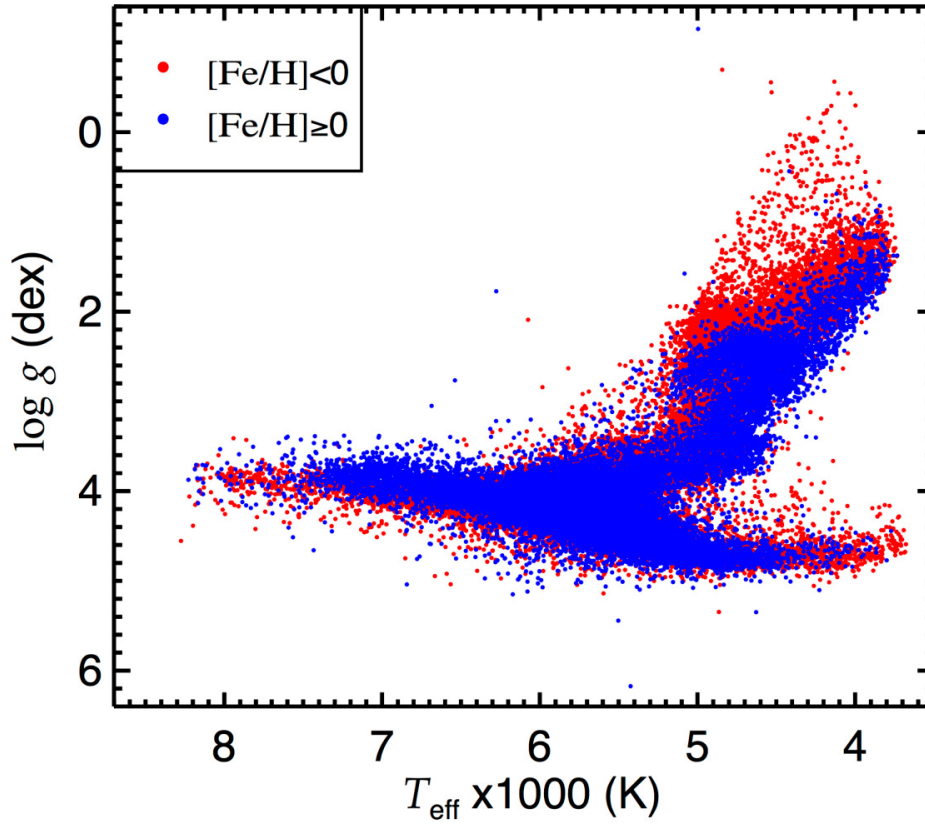


Fig. 7.— The position of the analyzed targets in a Kiel diagram ($\log g$ vs. T_{eff}) based on the calibrated stellar atmospheric parameters derived with LASP from the spectra obtained in the LK-project. The colors denote different values of $[\text{Fe}/\text{H}]$ (see legend in the top left corner).

peaks, which is a reflection of the main-sequence and the red giant branch, are shown in the histograms of T_{eff} and $\log g$ in Fig. 8(a) and (b), respectively. The distribution of $[\text{Fe}/\text{H}]$, as shown in Fig. 8(c), peaks near solar metallicity but is left-skewed with a tail that stretches away from the centre. As metal-deficient stars provide fundamental information of the chemical abundance formation and evolution from the early stage of the galaxy (Li et al. 2010; Deng et al. 2012), they are regarded as fossils of the early generation of stars. Based on the nomenclature for stars of different metallicity (Beers & Christlieb 2005) and the visual scan through 475 spectra with $[\text{Fe}/\text{H}] < -1.0$ dex, we finally classified 106 targets as candidate metal-poor stars (MPs, $[\text{Fe}/\text{H}] < -1.0$ dex) and 9 targets as candidate very metal-poor stars (VMPs, $[\text{Fe}/\text{H}] < -2.0$ dex). As shown in Fig. 8(d), the peak of the v_{rad} distribution deviates from 0 km s^{-1} and the mean value of the v_{rad} is -27.72 km s^{-1} . After scanning visually the spectra of 62 stars with $v_{\text{rad}} < -300 \text{ km/s}$ in the catalogue of the LK-project, only 18 stars were classified as candidate high-velocity stars (HVs) to study their natures and formation mechanisms, and to help improving our understanding of the structural properties of the galaxy. All the that are classified as a particular object are listed in the Table 5.

Note that most targets whose parameter values meet the conditions of the particular objects (MPs, VMPs and HVs) were rejected as candidates after a visual inspection of the data mainly due to the problems of the LAMOST spectra as already mentioned in Gray et al. (2016). For most LAMOST spectra, the background subtraction could be improved, but some spectra still exhibit negative flux values in some of their spectral lines. For spectra with an insufficient background subtraction, the determination of the parameters will also be inaccurate. Some spectra have low SNR values due to the low observed fluxes which makes it difficult to use the noisy spectral features for stellar parameter determinations. All the stars with LAMOST spectra suffering from at least one of these issues could not be retained as a candidate peculiar object. Most extreme values are usually derived from

the problematic spectra which are ascribed to the sorts of problems as given above. For this reason, the relative number of ‘wrong’ values for the parameters would be higher if we are looking at the extreme values (like the extremely low metallicities and extremely fast moving stars). Just because such stars are rare and we don’t expect many of them, and hence such values in the results can be indicative of errors in the analysis. The latest LAMOST reduction and analysis pipeline has been applied in an attempt to solve the problems. Satisfyingly, we estimate that only about 2% spectra are affected by the above mentioned problems in the LK-project after the quality of the spectra in four selected plates, which are observed on 2013/05/22, 2013/10/17, 2014/05/20 and 2014/09/17, have been visually checked.

7. Comparison with KIC

The KIC parameters were mostly derived from the multi-band photometric observations using a set of Sloan filters. This method is less reliable compared to parameter determination from spectroscopic data. The shortcomings of the KIC parameters have already been indicated in several previous works ([Hekker et al. 2011](#); [Brown et al. 2011](#); [Dong et al. 2014](#); [Liu et al. 2014](#)). Due to several known systematic defects ([Brown et al. 2011](#)), the accuracy of the atmospheric parameters as given in the KIC cannot reach the requirements for asteroseismic studies in many cases. As the main goal of the LK-project is to provide more accurate stellar parameters for objects in the KIC, we examined the reliability of stellar atmospheric parameters in the KIC by comparing them to the calibrated parameters that we obtained for stars in the LK-project.

There are 51,399 targets in the catalog of calibrated LAMP stellar atmospheric parameters (Table 4) that can be identified with an object from the KIC. However, stellar atmospheric parameters are listed in the KIC for only 41,775 of them. Figure 9 shows the

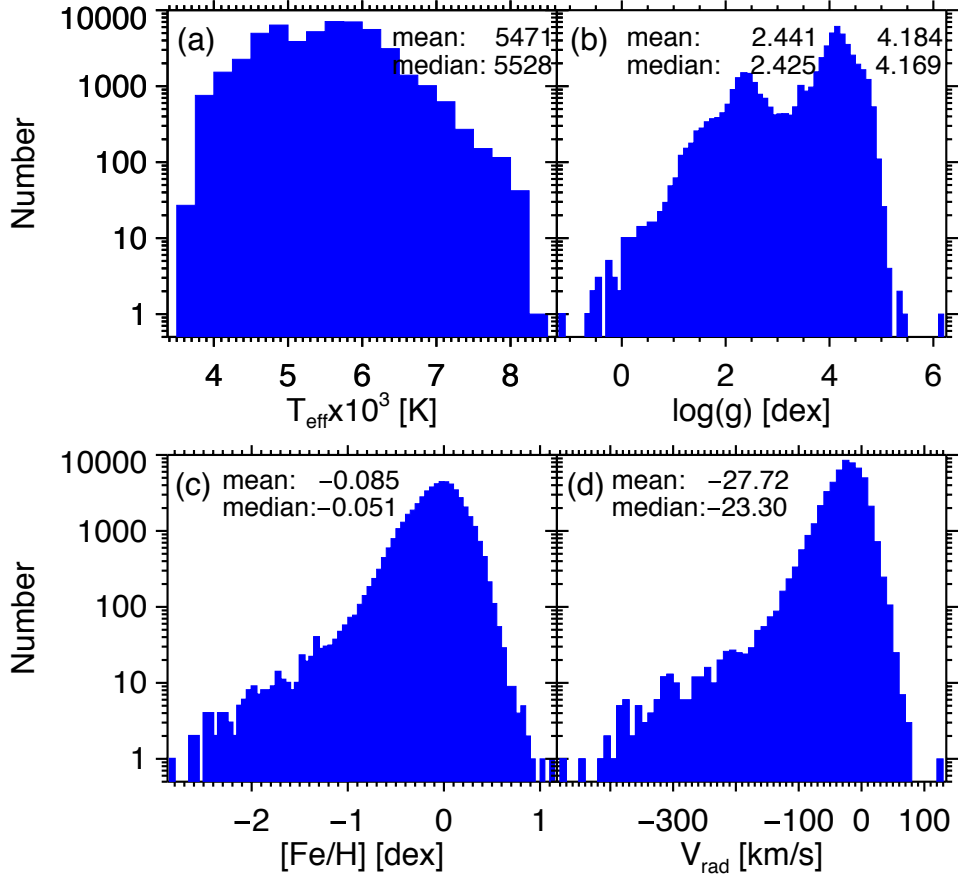


Fig. 8.— The histogram distribution of the 51,399 *Kepler* targets in (a) T_{eff} (250 K per bin), (b) $\log g$ (0.1 dex per bin), (c) $[\text{Fe}/\text{H}]$ (0.05 per bin) and (d) v_{rad} (10 km/s per bin). We calculate a set of mean and median values of these parameters. Two sets of mean and median values of the $\log g$ are given for the two parts with a cut-off point at $\log g = 3.5$ dex.

comparisons between the LASP and KIC parameters. It is clear from each of the upper panels that a lot of data points deviate from the 1:1 relation with a large scatter. All data points are divided into several bins with the bin size 500 K (for dwarfs) or 200 K (for giants) for T_{eff} , 0.2 dex for $\log g$ and 0.1 dex for $[\text{Fe}/\text{H}]$. If the number of data points in the bin is more than 200, the mean values and standard deviations of these data are represented by filled green circles and outer error bars, respectively. For the other bins, the mean values of the data are given by grey triangles. The black inner error bars give the standard deviation of the mean. The reliable filled green circles were fitted by straight lines or curve in Figure 9.

The linear relation of T_{eff} between the LK-project and KIC is satisfactory for most stars, although there are large discrepancies for a small portion of data in Figure 9 (a, d). There are no obvious differences in the quality of the T_{eff} measurements for dwarf and giant stars except that the KIC overestimates T_{eff} for most giant stars in the low temperature range. Even though the reliability of the LASP parameters has not been proven for stars with $T_{\text{eff}} > 7000$ K for dwarfs, we still observe a close relation between the T_{eff} values of both catalogues. A linear fit of the green points restricted, almost entirely, to the range with reliable LASP T_{eff} values (see Section 5.1; given in pink on Figure 9) leads to the following relations:

$$\begin{cases} T_{\text{eff,KIC}} = (0.898 \pm 0.003)T_{\text{eff,LASP}} + (0.529 \pm 0.016) \text{ (for giants)} \\ T_{\text{eff,KIC}} = (0.889 \pm 0.003)T_{\text{eff,LASP}} + (0.748 \pm 0.015) \text{ (for dwarfs)}, \end{cases} \quad (13)$$

where the subscript ‘KIC’ indicates the values originating from the KIC.

In Figure 9 (b, e), the comparisons of the $\log g$ values are given for giant and dwarf stars, respectively. There is a large dispersion around the bisector in the upper panels. Hence, for giants, we divided the filled green circles into three regions to fit these points

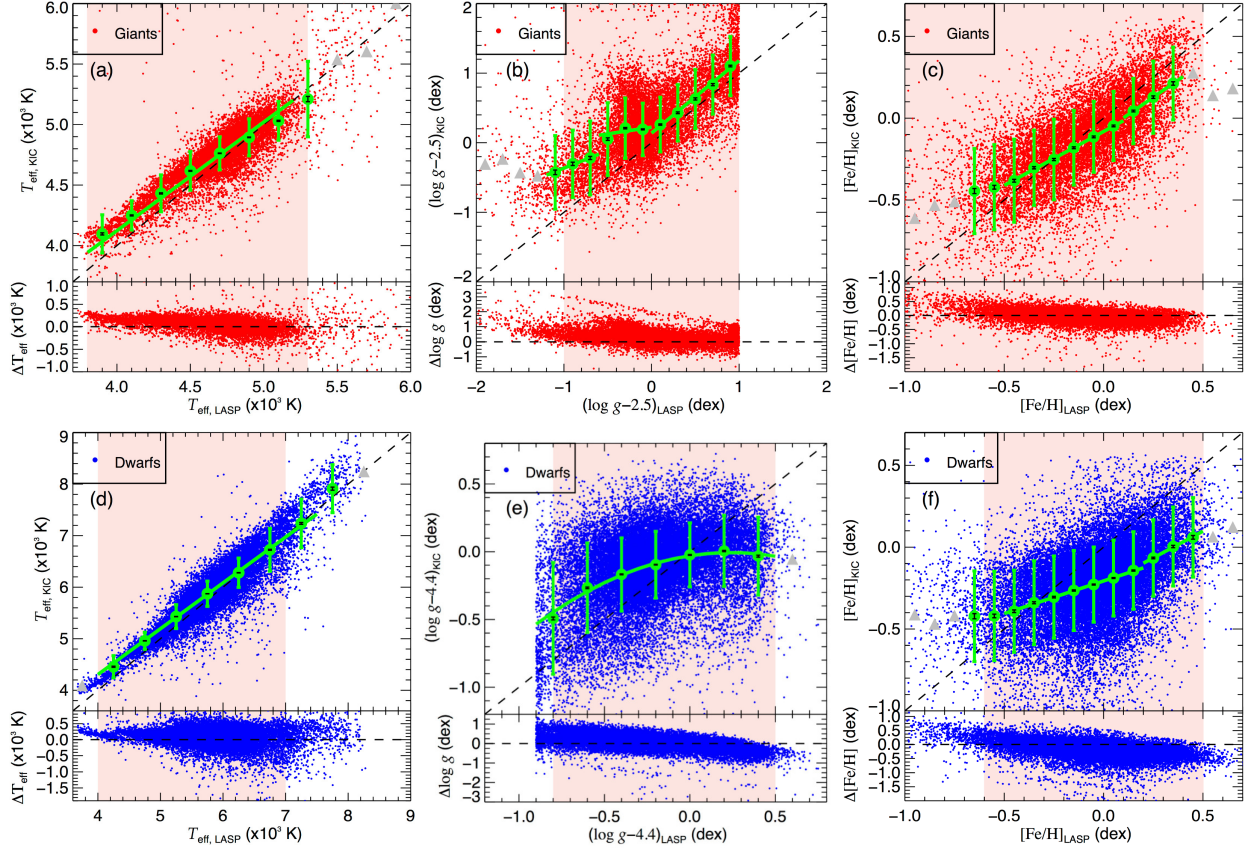


Fig. 9.— Comparison of the calibrated T_{eff} , $\log g$ and $[\text{Fe}/\text{H}]$ as determined by LASP (LASP X-axis) with those from KIC (KIC, Y-axis of the upper panels). In the upper panels, the common stars between the two datasets are plotted with red points for giant stars ($\log g < 3.5$ dex) and blue points for dwarf stars ($\log g \geq 3.5$). The green filled circles represent the mean values of each bin with at least 200 data points. The size of each bin is 500 K (for dwarfs) or 200 K (for giants) for T_{eff} , 0.2 dex for $\log g$ and 0.1 dex for $[\text{Fe}/\text{H}]$. The mean values of bins with less than 200 data points are given with grey triangles. The black dashed lines show the 1:1 relations while the green solid line are linear fits to the selected green filled circles. The outer error bars give the standard deviations and the black inner error bars give the standard deviation of the mean. In the lower panels, the difference (KIC - LASP) for these parameters are plotted in the Y-axis. The zero value is indicated by the black dashed line. The regions for which the reliability of the LASP parameters has been verified by the external calibration in Section 5.1 are indicated with a background in pink.

with a linear relationship, the fitting expression is given as follow:

$$\left\{ \begin{array}{l} (\log g - 2.5)_{\text{KIC}} = (0.502 \pm 0.097)(\log g - 2.5)_{\text{LASP}} + (0.137 \pm 0.084) \quad (\log g \in [1.3, 1.9]) \\ (\log g - 2.5)_{\text{KIC}} = (0.193 \pm 0.042)(\log g - 2.5)_{\text{LASP}} + (0.223 \pm 0.010) \quad (\log g \in [1.9, 2.5]) \\ (\log g - 2.5)_{\text{KIC}} = (1.042 \pm 0.017)(\log g - 2.5)_{\text{LASP}} + (0.138 \pm 0.010) \quad (\log g \in [2.5, 3.5]). \end{array} \right. \quad (14)$$

For dwarfs, we fitted all points with a quadratic polynomial in the 3.5-4.9 dex range as follows:

$$(\log g - 4.4)_{\text{KIC}} = (-0.406 \pm 0.017)(\log g - 4.4)_{\text{LASP}}^2 + (0.196 \pm 0.008)(\log g - 4.4)_{\text{LASP}} - (0.030 \pm 0.002). \quad (15)$$

The scatter of the KIC $\log g$ in the individual bins is about 0.426 and 0.292 dex for giants and dwarfs, respectively. The biases of the $\log g$ values mainly come from the large uncertainties of $\log g$ in KIC. This is mainly due to the shortcomings of the KIC stellar parameters. The primary goal of the KIC is to be able to distinguish the cool giant stars from the dwarf stars but the $\log g$ values are not accurate enough for asteroseismic studies (Brown et al. 2011). The KIC $\log g$ values are generally larger than the LASP values for most dwarf and giant stars, but KIC underestimate the $\log g$ in the range $\log g > 4.4$ dex for most dwarfs, and we can find an obvious deviation belt from 0.5 dex to about 2.5 dex for giant stars in the lower panel of Figure 9(b).

The situation when comparing $[\text{Fe}/\text{H}]$ values between the two datasets is even worse as can be seen on Figure 9 (c, f). The scatter of the KIC $[\text{Fe}/\text{H}]$ is about 0.223 and 0.242 dex for giants and dwarfs in the individual bins, respectively. This situation should be mainly ascribed to problems of the KIC (Plavchan et al. 2014). There is also an obvious wide deviation for most giant and dwarf stars: the KIC seriously overestimates the $[\text{Fe}/\text{H}]$ values for most metal poor stars, but it underestimates the $[\text{Fe}/\text{H}]$ values for most stars around 0 dex, as mentioned in Dong et al. (2014), especially for dwarfs. Finally, we divided the green points into two ranges to separately fit them with a linear function. We give the resulting

relations for giants:

$$\left\{ \begin{array}{l} [\text{Fe}/\text{H}]_{\text{KIC}} = (0.659 \pm 0.015)[\text{Fe}/\text{H}]_{\text{LASP}} - (0.081 \pm 0.003) \quad ([\text{Fe}/\text{H}] \in [-0.5, 0.1]) \\ [\text{Fe}/\text{H}]_{\text{KIC}} = (0.842 \pm 0.055)[\text{Fe}/\text{H}]_{\text{LASP}} - (0.083 \pm 0.012) \quad ([\text{Fe}/\text{H}] \in [0.1, 0.4]) \end{array} \right. \quad (16)$$

and dwarfs:

$$\left\{ \begin{array}{l} [\text{Fe}/\text{H}]_{\text{KIC}} = (0.400 \pm 0.010)[\text{Fe}/\text{H}]_{\text{LASP}} - (0.206 \pm 0.002) \quad ([\text{Fe}/\text{H}] \in [-0.5, 0.2]) \\ [\text{Fe}/\text{H}]_{\text{KIC}} = (0.651 \pm 0.055)[\text{Fe}/\text{H}]_{\text{LASP}} - (0.228 \pm 0.017) \quad ([\text{Fe}/\text{H}] \in [0.2, 0.5]) \end{array} \right. \quad (17)$$

to calibrate the parameters in the KIC.

8. Conclusions and Prospects

The low-resolution spectroscopic observations for the stars in the *Kepler* field with LAMOST were started at Xinglong observatory on May 30, 2011. There are 88,628 flux- and wavelength-calibrated, sky-subtracted spectra to be released in the third data release (DR3) of LAMOST. These spectra were obtained in the observation seasons from June 2012 to September 2014. After three years of discontinuous observations, 14 LK-fields covering the whole *Kepler*-field have been observed discontinuously at 25 nights. Based on the LASP stellar parameters, we derived the analysis stellar atmospheric parameters (T_{eff} , $\log g$, $[\text{Fe}/\text{H}]$), the radial velocity (v_{rad}) and their errors for 51,406 stars from 61,226 late A, F, G and K type stars having at least one LAMOST spectrum with $\text{SNR}_g \geq 6.0$ in the catalog of the LK-project. The magnitude distribution of these objects mainly ranges from 11 to 15 magnitude. Among the 51,406 observed stars, more than half (30,110) were observed photometrically by the Kepler mission in the *Kepler* field. As 8,632 targets have been observed more than once, the ratio of multiple observation stars is close to 17%. The wrong IDs of 9 fibers of spectrograph 4 affect 71 spectra in the LK-project since the start of the survey in June 2012. We have corrected the ID of these spectra according to the latest updated information in the LAMOST DR2 website.

The comparison of the LASP parameters with the T_{eff} and $[\text{Fe}/\text{H}]$ derived from high-resolution ($R \geq 20,000$) spectra and the $\log g$ calculated by the means of asteroseismology given in six subsamples in HT4 offers an effective method to perform the external calibration of the parameters from the LK-project. Using the atmospheric parameters and their errors of the common giant and dwarf stars in the two data sets, close to 1:1 linear relations are found as best fits for T_{eff} , $\log g$, and $[\text{Fe}/\text{H}]$, respectively. Almost all data points are located in the 3σ confidence intervals of the residual parameters. The mean deviation (LASP - Huber) and the external uncertainties of T_{eff} , $\log g$ and $[\text{Fe}/\text{H}]$ are 34 ± 131 K, 0.13 ± 0.19 dex and -0.04 ± 0.15 dex for the giants, 5 ± 104 K, -0.05 ± 0.16 dex and -0.01 ± 0.10 dex for the dwarfs, respectively. We showed that the LASP parameters of the stars in our catalogue are reliable in the ranges of 3,800 to 5,300 K for T_{eff} , 1.5 to 3.5 dex for $\log g$, and -1.0 to 0.5 dex for $[\text{Fe}/\text{H}]$ for giant stars, 4,000 to 7,000 K for T_{eff} , 3.6 to 4.9 dex for $\log g$, and -0.6 to 0.5 dex for $[\text{Fe}/\text{H}]$ for dwarf stars, respectively. These ranges are not the same for giant and dwarf stars, as shown in the pink background regions of Figure 9. Using the unbiased estimated method, we estimated the internal errors of the LASP parameters with $\text{SNR}_g \geq 6.0$ based on the stars with multiple LAMOST spectra: 91 K, 0.12 dex and 0.09 dex for T_{eff} , $\log g$ and $[\text{Fe}/\text{H}]$, respectively. The internal uncertainties of stellar parameters are defined with second-order polynomials as a function of SNR_g . Finally, the LASP stellar parameters and their errors were calibrated by taking both internal and external calibration into account.

For the analysis of the overall distributions of the calibrated atmospheric parameters and radial velocities to search for particular stars, we considered the LASP parameters derived from the LAMOST spectra with the highest SNR_g value for stars with multiple observations. No special objects were found from the analysis of the effective temperature and the surface gravity. However, 106 stars could be classified as candidate MPs and 9 as candidate VMPs from the sample of stars with $[\text{Fe}/\text{H}] < -1.0$ dex after visual inspection of

the results. Moreover, 18 stars from the sample of targets with $v_{\text{rad}} < -300$ km/s in *Kepler* field can be considered as candidate HVs.

There are 51,399 common stars between the LASP catalogue and the KIC. For 41,775 of them, atmospheric parameters are listed in the KIC. Issues with the KIC parameters, especially for $\log g$ and $[\text{Fe}/\text{H}]$, are confirmed by the comparison with the calibrated parameters derived within the LK-project. The KIC overestimates the parameters for most of giants but underestimates the $[\text{Fe}/\text{H}]$ values in the range of $[\text{Fe}/\text{H}] > -0.2$ dex. All the parameters in the KIC can be calibrated by applying the correlations between LASP and KIC values as given in Section 7. The missing atmospheric parameters for 9,624 stars in the KIC can now be replaced for the majority of them by the calibrated LASP parameters within the reliable ranges (3,800 \sim 7,000 K for T_{eff} , 1.5 \sim 4.9 dex for $\log g$, and -1.0 \sim 0.5 dex for $[\text{Fe}/\text{H}]$).

The stellar parameters determined by the LASP based on the normalized low-resolution spectra of the LK-project are available for LAMOST users from on the world wide web: <http://dr3.lamost.org>. The reduced spectra and stellar parameters will be released to the interested astronomers all over the world through the LAMOST official data release in June 2017. The calibrated stellar atmospheric parameters and the radial velocities obtained within the LK-project are helpful for various studies of stars in the *Kepler* field. Although plenty of the stars that have been observed by the *Kepler* mission were not observed yet during the first round of observations, a good progress has been made in 2015 as 32 additional plates, covering the whole *Kepler* field except for one subfield (LK01), have been observed during 18 nights. The observations for the LK-project are still ongoing. Moreover, a proposal for LAMOST observations for six K2 mission fields with the declination higher than -10 deg (Howell et al. 2014) has been approved and started to carry out. We therefore expect to obtain many more high-quality spectroscopic observations with the LAMOST for

stars in both the *Kepler* field and fields of the K2 mission in near future.

Table 4. The catalog of calibrated LASP stellar atmosphere parameters in the first round of observations for the LK-project.

Obsid	Target	SNR _g	Subclass	T _{eff} (K)	log g (dex)	[Fe/H] (dex)
52201011	KIC07042868	76.73	G5	4844±149	2.485±0.211	0.031±0.165
52201018	KIC06957157	50.72	G5	4727±155	2.284±0.220	0.051±0.173
52201025	KIC06957977	47.57	K1	4758±156	1.994±0.222	-0.189±0.174
52201040	KIC07206837	46.50	F6	6183±134	4.167±0.198	0.230±0.134
52201060	KIC07368371	98.09	K3	4114±146	1.705±0.206	-0.121±0.162
...
250016240	KIC12933001	25.87	K1	4802±149	3.967±0.223	0.044±0.155
250016244	KIC12983407	20.10	G8	5448±158	4.386±0.236	-0.019±0.166
250016245	KIC12883530	102.95	F0	7022±122	4.003±0.178	-0.003±0.116
250016248	KIC12933571	19.47	K5	4448±178	2.510±0.259	-0.227±0.202
250016249	KIC12883443	18.22	K0	5086±161	3.742±0.242	0.036±0.171

Table 5. The calibrated LASP atmosphere parameters (T_{eff} , $\log g$ and $[\text{Fe}/\text{H}]$) and the LASP radial velocity (v_{rad}) for the candidates of the particular objects in the LK-project. The spectra of these candidates were inspected visually to ensure the reliability of these candidates.

Obsid	Target	SNR _g	Subclass	T_{eff} (K)	$\log g$ (dex)			
243016087	KIC06022596	57.54	F2	5176 ± 108	2.421 ± 0.153	-1.728 ± 0.120	-130.59 ± 39.95	MPs
243116087	KIC06022596	56.15	F2	5208 ± 108	2.480 ± 0.154	-1.702 ± 0.121	-128.07 ± 38.60	MPs
163007106	KIC06022596	46.66	F2	5221 ± 110	2.496 ± 0.157	-1.719 ± 0.123	-134.74 ± 31.90	MPs
238003154	KIC09933034	109.00	F0	6232 ± 86	4.255 ± 0.126	-1.143 ± 0.082	-123.38 ± 39.38	MPs
242703154	KIC09933034	81.51	F0	6262 ± 88	4.289 ± 0.129	-1.132 ± 0.085	-124.43 ± 41.80	MPs
242603154	KIC09933034	18.03	F0	6226 ± 114	4.192 ± 0.172	-1.173 ± 0.121	-123.70 ± 42.52	MPs
154015047	KIC08162514	66.86	G5	4431 ± 106	1.106 ± 0.151	-1.289 ± 0.118	-73.82 ± 17.77	MPs
155015047	KIC08162514	49.99	G8	4474 ± 109	1.198 ± 0.156	-1.225 ± 0.122	-77.47 ± 18.08	MPs
159612061	KIC08364751	234.41	F0	6244 ± 83	4.232 ± 0.120	-1.098 ± 0.076	-296.47 ± 35.32	MPs
247610021	KIC08364751	79.37	F3	6192 ± 88	4.257 ± 0.130	-1.237 ± 0.085	-304.03 ± 38.02	MPs
170509015	KIC09432243	113.34	F0	5867 ± 86	4.030 ± 0.125	-1.944 ± 0.081	-161.10 ± 50.09	MPs
165909015	KIC09432243	51.26	F0	5884 ± 93	4.057 ± 0.138	-1.953 ± 0.093	-158.96 ± 47.14	MPs
238004170	KIC09813342	165.85	G0	5657 ± 84	4.315 ± 0.122	-1.328 ± 0.078	-172.55 ± 29.48	MPs
242604170	KIC09813342	116.47	G0	5648 ± 86	4.308 ± 0.125	-1.339 ± 0.081	-171.77 ± 31.47	MPs
249201249	KIC09818964	73.31	G2	4923 ± 105	2.085 ± 0.150	-1.662 ± 0.117	-200.73 ± 28.13	MPs
242706043	KIC09818964	45.82	G3	4880 ± 110	1.783 ± 0.158	-1.702 ± 0.124	-205.47 ± 28.89	MPs
247611205	KIC09956941	73.33	F7	5907 ± 89	4.068 ± 0.131	-1.849 ± 0.087	-285.20 ± 37.92	MPs
241006143	KIC09956941	48.83	F0	5890 ± 94	4.055 ± 0.139	-1.855 ± 0.094	-284.24 ± 43.81	MPs
238015073	KIC10319045	215.86	G5	4432 ± 100	1.228 ± 0.141	-1.077 ± 0.110	-126.78 ± 16.73	MPs
242615073	KIC10319045	150.78	G5	4430 ± 101	1.207 ± 0.142	-1.071 ± 0.111	-128.31 ± 16.78	MPs
242612192	KIC11017176	90.15	G7	4847 ± 104	1.506 ± 0.147	-1.474 ± 0.115	-226.61 ± 24.90	MPs
238012192	KIC11017176	68.40	G7	4914 ± 106	1.660 ± 0.151	-1.376 ± 0.118	-229.65 ± 25.02	MPs
157214098	KIC11457596	58.31	F0	6066 ± 92	4.158 ± 0.135	-1.492 ± 0.090	-285.17 ± 47.70	MPs
248606006	KIC11457596	47.75	F0	6300 ± 94	4.273 ± 0.139	-1.377 ± 0.094	-286.85 ± 37.38	MPs
248610109	KIC11704816	59.59	G2	5089 ± 107	2.416 ± 0.153	-1.624 ± 0.120	-180.04 ± 25.69	MPs
249610109	KIC11704816	17.24	G2	5162 ± 128	2.903 ± 0.188	-1.569 ± 0.146	-183.21 ± 22.67	MPs
249209055	KIC11857234	52.26	G3	4749 ± 109	1.683 ± 0.155	-1.370 ± 0.122	-108.28 ± 17.06	MPs
248610023	KIC11857234	35.12	G3	4680 ± 114	1.624 ± 0.164	-1.445 ± 0.128	-110.76 ± 20.65	MPs
52507223	KIC01580348	32.90	G3	4635 ± 115	1.122 ± 0.166	-1.670 ± 0.130	-316.10 ± 22.83	MPs
243006015	KIC03838579	59.70	F2	5928 ± 91	4.204 ± 0.134	-1.036 ± 0.090	-93.67 ± 28.97	MPs
243104137	KIC04446192	132.63	F7	5827 ± 85	4.303 ± 0.124	-1.240 ± 0.080	-70.27 ± 36.89	MPs

Table 5—Continued

Obsid	Target	SNR _g	Subclass	T _{eff} (K)	log g (dex)			
243013134	KIC05176287	16.23	K1	4597 ± 130	2.392 ± 0.191	-1.074 ± 0.148	-45.26 ± 17.52	MPs
159601033	KIC05268275	102.09	F2	5791 ± 86	4.357 ± 0.126	-1.049 ± 0.082	-7.73 ± 31.64	MPs
154001194	KIC05271670	32.19	G2	5537 ± 101	4.453 ± 0.150	-1.047 ± 0.103	-7.77 ± 27.57	MPs
154007230	KIC05362244	46.72	F5	6017 ± 95	4.253 ± 0.140	-1.062 ± 0.095	-104.87 ± 32.72	MPs
163002116	KIC05422924	31.15	G2	5191 ± 116	2.897 ± 0.168	-1.390 ± 0.131	-77.31 ± 32.11	MPs
243114093	KIC05513197	37.08	G2	5115 ± 113	2.303 ± 0.163	-1.138 ± 0.127	-83.83 ± 30.56	MPs
163002084	KIC05933607	44.88	G3	4962 ± 111	2.282 ± 0.158	-1.045 ± 0.124	-210.33 ± 24.51	MPs
243112023	KIC05948716	49.52	F0	6308 ± 94	4.129 ± 0.138	-1.382 ± 0.093	-384.46 ± 44.13	MPs
52815099	KIC05966097	26.00	F3	6142 ± 105	4.204 ± 0.157	-1.505 ± 0.109	-373.05 ± 40.29	MPs
154002171	KIC06111652	63.90	G5	4674 ± 107	1.715 ± 0.152	-1.024 ± 0.119	-16.79 ± 20.34	MPs
163005015	KIC06263778	42.56	G3	4902 ± 111	2.179 ± 0.159	-1.319 ± 0.125	-292.35 ± 25.34	MPs
161401216	KIC06271226	56.32	G6	4721 ± 108	1.326 ± 0.154	-1.372 ± 0.121	-65.14 ± 21.75	MPs
162314060	KIC06533598	11.14	G7	4639 ± 129	4.331 ± 0.196	-1.187 ± 0.140	-19.61 ± 21.82	MPs
159608008	KIC06604237	130.46	G3	4646 ± 102	1.307 ± 0.143	-1.884 ± 0.112	-330.28 ± 30.71	MPs
159610225	KIC06766131	53.09	F2	5793 ± 93	3.883 ± 0.137	-1.013 ± 0.092	-104.06 ± 38.28	MPs
159603018	KIC06769852	60.43	G0	5432 ± 107	3.272 ± 0.153	-1.122 ± 0.120	-222.36 ± 27.77	MPs
161402195	KIC07263702	32.33	F6	5782 ± 101	4.273 ± 0.150	-1.199 ± 0.103	-22.24 ± 40.14	MPs
163004071	KIC07505345	43.02	F0	6664 ± 96	4.251 ± 0.142	-1.010 ± 0.096	-235.09 ± 34.11	MPs
161410216	KIC07590793	33.56	G6	5156 ± 100	4.533 ± 0.149	-1.268 ± 0.102	-260.26 ± 21.75	MPs
247605091	KIC07614421	26.60	G3	4969 ± 119	2.135 ± 0.172	-1.660 ± 0.134	-243.66 ± 27.27	MPs
161410078	KIC07665025	37.05	G3	5024 ± 113	2.419 ± 0.163	-1.301 ± 0.127	-277.68 ± 27.26	MPs
170501034	KIC07917764	59.51	G3	4829 ± 107	1.670 ± 0.153	-1.256 ± 0.120	-34.16 ± 25.81	MPs
163015114	KIC07940280	67.72	F0	6016 ± 90	4.192 ± 0.132	-1.302 ± 0.088	-293.76 ± 37.00	MPs
161404092	KIC07948268	90.16	G2	5154 ± 104	2.870 ± 0.147	-1.196 ± 0.115	-296.78 ± 26.41	MPs
161408041	KIC08019664	26.97	G3	4993 ± 119	2.287 ± 0.172	-1.433 ± 0.134	-392.03 ± 29.72	MPs
163015138	KIC08077380	72.41	G2	5373 ± 89	3.565 ± 0.131	-1.090 ± 0.087	-179.12 ± 25.33	MPs
163013110	KIC08082012	33.85	G5	4481 ± 115	1.100 ± 0.165	-1.175 ± 0.129	-203.86 ± 17.00	MPs
247603025	KIC08237832	50.14	F6	5919 ± 94	3.658 ± 0.138	-1.126 ± 0.093	-233.69 ± 24.69	MPs
163016116	KIC08409682	34.82	G8	5079 ± 100	4.786 ± 0.148	-1.363 ± 0.101	-45.90 ± 19.19	MPs
163012135	KIC08412954	39.96	G2	5129 ± 112	2.594 ± 0.161	-1.939 ± 0.126	-285.53 ± 37.45	MPs
163011233	KIC08476245	24.69	G3	4977 ± 120	2.059 ± 0.175	-1.035 ± 0.136	-124.18 ± 20.85	MPs

Table 5—Continued

Obsid	Target	SNR _g	Subclass	T _{eff} (K)	log g (dex)			
161415241	KIC08612146	29.59	G3	4857 ± 117	1.778 ± 0.169	−1.821 ± 0.132	−196.22 ± 29.30	MPs
242607068	KIC08869235	47.17	G6	5014 ± 110	2.607 ± 0.157	−1.020 ± 0.123	−217.90 ± 20.56	MPs
242602239	KIC08999218	59.87	F0	6114 ± 91	4.218 ± 0.134	−1.153 ± 0.090	−64.38 ± 40.37	MPs
242707109	KIC09004948	58.37	G6	4954 ± 108	2.115 ± 0.153	−1.718 ± 0.120	−252.13 ± 29.68	MPs
238005009	KIC09071237	105.14	G5	5293 ± 86	4.552 ± 0.126	−1.211 ± 0.082	−264.42 ± 21.28	MPs
241007071	KIC09156667	43.72	F2	5515 ± 96	3.756 ± 0.141	−1.629 ± 0.096	−265.32 ± 35.29	MPs
158804247	KIC09245734	90.99	F5	5874 ± 87	3.971 ± 0.128	−1.580 ± 0.084	−44.44 ± 41.96	MPs
158814069	KIC09358384	48.54	A6IV	6568 ± 94	4.368 ± 0.139	−1.218 ± 0.094	3.45 ± 40.35	MPs
238006155	KIC09452906	26.52	F5	6062 ± 105	4.173 ± 0.156	−1.177 ± 0.109	−15.66 ± 35.28	MPs
158804038	KIC09610507	33.59	G2	5648 ± 100	3.802 ± 0.149	−1.001 ± 0.102	−6.84 ± 30.35	MPs
242606141	KIC09637337	129.71	G3	5055 ± 102	2.681 ± 0.143	−1.007 ± 0.112	−143.79 ± 22.08	MPs
242608054	KIC09696716	135.81	G3	4944 ± 102	2.088 ± 0.143	−1.479 ± 0.112	−154.07 ± 28.61	MPs
247711176	KIC09836233	33.43	K3	4836 ± 100	4.768 ± 0.149	−1.035 ± 0.102	−141.19 ± 12.74	MPs
249207177	KIC10398120	162.33	G5	4686 ± 101	1.620 ± 0.142	−1.002 ± 0.111	−206.11 ± 13.10	MPs
242613111	KIC10521392	68.65	F5	6002 ± 90	4.179 ± 0.132	−1.059 ± 0.088	−13.37 ± 33.87	MPs
249601024	KIC10729186	22.96	G7	5156 ± 122	3.161 ± 0.177	−1.087 ± 0.138	−83.42 ± 18.34	MPs
154803010	KIC10737052	35.70	G4	4954 ± 114	2.233 ± 0.164	−1.266 ± 0.128	−252.20 ± 25.11	MPs
249601045	KIC10858420	11.44	G7	5281 ± 128	4.023 ± 0.194	−1.089 ± 0.139	−119.22 ± 15.94	MPs
241009055	KIC10920437	71.12	G2	5241 ± 106	2.839 ± 0.150	−1.271 ± 0.118	−159.40 ± 26.72	MPs
157213090	KIC11044756	27.47	F6	5645 ± 104	3.900 ± 0.155	−1.227 ± 0.108	−242.86 ± 28.43	MPs
157214239	KIC11296574	109.35	G0	5580 ± 86	3.848 ± 0.125	−1.160 ± 0.081	−260.01 ± 34.63	MPs
249213204	KIC11345077	37.45	G3	5104 ± 113	2.726 ± 0.163	−1.255 ± 0.127	−245.21 ± 20.36	MPs
250006172	KIC11563791	129.19	G6	4947 ± 102	2.446 ± 0.143	−1.092 ± 0.112	−269.72 ± 19.00	MPs
248603228	KIC11757807	117.74	F9	4659 ± 102	1.522 ± 0.144	−1.388 ± 0.113	−220.34 ± 18.30	MPs
249215021	KIC11855373	80.07	A6IV	6648 ± 88	4.362 ± 0.129	−1.466 ± 0.085	−243.65 ± 26.38	MPs
249215154	KIC11953764	75.52	G3	5169 ± 105	3.010 ± 0.149	−1.053 ± 0.117	−177.25 ± 19.89	MPs
249211077	KIC12004528	76.55	F0	6202 ± 89	4.117 ± 0.130	−1.785 ± 0.086	−199.49 ± 41.33	MPs
249613052	KIC12017985	53.65	G3	4941 ± 109	2.143 ± 0.155	−1.754 ± 0.121	−200.09 ± 26.24	MPs
249216059	KIC12051330	86.01	G3	4916 ± 104	2.120 ± 0.147	−1.435 ± 0.116	−69.32 ± 20.47	MPs
248604206	KIC12207740	137.58	G6	4948 ± 102	2.361 ± 0.143	−1.127 ± 0.112	−11.63 ± 20.50	MPs
249609181	KIC12210298	38.81	F0	6413 ± 98	4.261 ± 0.145	−1.342 ± 0.099	−169.33 ± 31.90	MPs

Table 5—Continued

Obsid	Target	SNR _g	Subclass	T _{eff} (K)	log g (dex)			
157211215	KIC12216301	63.31	G2	5220 ± 107	2.937 ± 0.152	−1.341 ± 0.119	−217.26 ± 29.95	MPs
248615245	KIC12304604	39.25	G0	5251 ± 113	2.985 ± 0.161	−1.305 ± 0.126	−182.56 ± 23.70	MPs
248615168	KIC12645981	88.89	F0	6514 ± 87	4.224 ± 0.128	−1.003 ± 0.084	−294.27 ± 28.49	MPs
238014090	KIC10383102	36.47	F0	5957 ± 99	3.676 ± 0.146	−2.257 ± 0.100	−150.17 ± 53.56	VMPs
242714090	KIC10383102	32.87	F0	5846 ± 101	3.704 ± 0.149	−2.192 ± 0.103	−153.54 ± 56.68	VMPs
247607120	KIC07693833	113.55	G2	4931 ± 102	1.982 ± 0.145	−2.292 ± 0.113	−13.08 ± 27.59	VMPs
242707138	KIC09006890	41.86	G2	4823 ± 112	1.829 ± 0.160	−2.236 ± 0.125	−270.85 ± 43.57	VMPs
248602055	KIC11080134	66.36	F0	5822 ± 90	3.626 ± 0.133	−2.133 ± 0.088	−266.92 ± 42.09	VMPs
<hr/>								
242603099	KIC09751081	85.62	G7	4782 ± 104	1.680 ± 0.148	−1.697 ± 0.116	−311.77 ± 27.01	HVs
242703076	KIC09751081	53.67	G7	4778 ± 109	1.674 ± 0.155	−1.719 ± 0.121	−309.25 ± 28.22	HVs
154007087	KIC05621880	34.48	G3	5582 ± 100	4.239 ± 0.148	−0.654 ± 0.102	−316.05 ± 20.27	HVs
159603161	KIC07191496	178.88	G6	4900 ± 101	1.968 ± 0.141	−1.983 ± 0.111	−305.52 ± 33.37	HVs
163014201	KIC07658030	26.07	G5	4303 ± 119	0.415 ± 0.173	−1.905 ± 0.135	−406.20 ± 23.55	HVs
242707005	KIC08802291	27.52	G8	4707 ± 118	1.495 ± 0.171	−1.775 ± 0.134	−308.53 ± 27.56	HVs
250007083	KIC11032723	31.34	G6	4606 ± 116	1.552 ± 0.167	−1.251 ± 0.131	−304.73 ± 13.96	HVs
249209210	KIC11395462	66.91	G6	4764 ± 106	2.194 ± 0.151	−0.764 ± 0.118	−328.13 ± 13.78	HVs
154811189	KIC12019793	20.46	G6	4888 ± 124	2.543 ± 0.181	−0.655 ± 0.141	−303.65 ± 18.96	HVs
<hr/>								
243009061	KIC05691816	52.75	G7	4957 ± 109	2.071 ± 0.155	−1.638 ± 0.121	−305.47 ± 31.85	MPs,HVs
154005087	KIC06116549	68.50	G2	4993 ± 106	2.260 ± 0.151	−1.799 ± 0.118	−359.86 ± 40.14	MPs,HVs
154008102	KIC06362206	142.61	F0	5995 ± 84	4.052 ± 0.123	−1.441 ± 0.079	−324.81 ± 39.04	MPs,HVs
154004124	KIC07030715	103.78	F0	6293 ± 86	4.194 ± 0.126	−1.332 ± 0.082	−336.47 ± 39.84	MPs,HVs
161405185	KIC07666893	35.28	G3	4542 ± 114	0.884 ± 0.164	−1.880 ± 0.128	−316.54 ± 25.42	MPs,HVs
154014085	KIC07673401	42.07	F0	5914 ± 96	3.989 ± 0.142	−1.699 ± 0.097	−305.13 ± 53.01	MPs,HVs
161409033	KIC08680868	27.97	G4	4926 ± 118	2.346 ± 0.171	−1.019 ± 0.133	−381.01 ± 20.66	MPs,HVs
241002039	KIC09335536	70.25	G6	4819 ± 106	1.670 ± 0.150	−1.576 ± 0.118	−356.46 ± 27.98	MPs,HVs
241004161	KIC10203516	119.67	F5	6026 ± 85	4.191 ± 0.125	−1.235 ± 0.081	−305.50 ± 38.29	MPs,HVs
249214199	KIC11336325	63.02	G5	4374 ± 107	0.936 ± 0.152	−1.250 ± 0.119	−326.35 ± 14.06	MPs,HVs

9. Acknowledgments

Guoshoujing Telescope (the Large Sky Area Multi-Object Fiber Spectroscopic Telescope LAMOST) is a National Major Scientific Project built by the Chinese Academy of Sciences. Funding for the project has been provided by the National Development and Reform Commission. LAMOST is operated and managed by the National Astronomical Observatories, Chinese Academy of Sciences. JNF acknowledges the support by the Joint Fund of Astronomy of National Science Foundation of China (NSFC) and Chinese Academy of Sciences through the grant U1231202 and the National Basic Research Program of China (973 program 2014CB845700 and 2013CB834900). The LAMOST FELLOWSHIP is supported by Special Funding for Advanced Users, budgeted and administrated by Center for Astronomical Mega-Science, Chinese Academy of Sciences (CAMS). YW acknowledges the NSFC under grant 11403056. SD is supported by the Strategic Priority Research Program-The Emergence of Cosmological Structures of the Chinese Academy of Sciences (Grant No. XDB09000000) and Project 11573003 supported by NSFC. ABR thanks Antonio Frasca, Joanna Molenda-Żakowicz and Gianni Catanzaro for helpful discussions.

REFERENCES

- Aoki, W. 2014, Subaru Proposal, 112
- Batalha, N. M., Rowe, J. F., Bryson, S. T., et al. 2013, *ApJS*, 204, 24
- Beers, T. C., & Christlieb, N. 2005, *ARA&A*, 43, 531
- Borucki, W. J., Koch, D., Jenkins, J., et al. 2009, *Science*, 325, 709
- Borucki, W. J., Koch, D. G., Lissauer, J., et al. 2007, *Transiting Extrapolar Planets Workshop*, 366, 309
- Brown, T. M., Latham, D. W., Everett, M. E., & Esquerdo, G. A. 2011, *AJ*, 142, 112
- Bruntt, H., Bedding, T. R., Quirion, P.-O., et al. 2010, *MNRAS*, 405, 1907
- Bruntt, H., Frandsen, S., & Thygesen, A. O. 2011, *A&A*, 528, A121
- Bruntt, H., Basu, S., Smalley, B., et al. 2012, *MNRAS*, 423, 122
- Buchhave, L. A., Latham, D. W., Johansen, A., et al. 2012, *Nature*, 486, 375
- Catanzaro, G., Frasca, A., Molenda-Żakowicz, J., & Marilli, E. 2010, *A&A*, 517, A3
- Catanzaro, G., Ripepi, V., Bernabei, S., et al. 2011, *MNRAS*, 411, 1167
- Chaplin, W. J., Appourchaux, T., Elsworth, Y., et al. 2010, *ApJ*, 713, L169
- Christensen-Dalsgaard, J., Arentoft, T., Brown, T. M., et al. 2007, *Communications in Asteroseismology*, 150, 350
- Creevey, O. L., Thévenin, F., Basu, S., et al. 2013, *MNRAS*, 431, 2419
- Cui, X.-Q., Zhao, Y.-H., Chu, Y.-Q., et al. 2012, *Research in Astronomy and Astrophysics*, 12, 1197

- De Cat, P., Fu, J., Yang, X., et al. 2014, arXiv:1411.0913
- De Cat, P., Fu, J. N., Ren, A. B., et al. 2015, *ApJS*, 220, 19
- Deng, L.-C., Newberg, H. J., Liu, C., et al. 2012, *Research in Astronomy and Astrophysics*, 12, 735
- Dong, S., Zheng, Z., Zhu, Z., et al. 2014, *ApJ*, 789, L3
- Epstein, C. 2015, *Astrophysics and Space Science Proceedings*, 39, 133
- Frasca, A., Alcalá, J. M., Covino, E., et al. 2003, *A&A*, 405, 149
- Gilliland, R. L., Brown, T. M., Christensen-Dalsgaard, J., et al. 2010, *PASP*, 122, 131
- Glazebrook, K., Offer, A. R., & Deeley, K. 1998, *ApJ*, 492, 98
- Gray, R. O., Corbally, C. J., De Cat, P., et al. 2016, *AJ*, 151, 13
- Hekker, S., Gilliland, R. L., Elsworth, Y., et al. 2011, *MNRAS*, 414, 2594
- Howell, S. B., Sobek, C., Haas, M., et al. 2014, *PASP*, 126, 398
- Huber, D., Chaplin, W. J., Christensen-Dalsgaard, J., et al. 2013, *ApJ*, 767, 127
- Huber, D., Silva Aguirre, V., Matthews, J. M., et al. 2014, *ApJS*, 211, 2
- Karoff, C., Metcalfe, T. S., Chaplin, W. J., et al. 2013, *MNRAS*, 433, 3227
- Kasting, J. F., Whitmire, D. P., & Reynolds, R. T. 1993, *Icarus*, 101, 108
- Lehmann, H., Tkachenko, A., Semaan, T., et al. 2011, *A&A*, 526, A124
- Li, H.-N., Zhao, G., Christlieb, N., et al. 2010, *Research in Astronomy and Astrophysics*, 10, 753

- Li, H.-N., Zhao, G., Christlieb, N., et al. 2015a, *ApJ*, 798, 110
- Li, H., Aoki, W., Zhao, G., et al. 2015b, *PASJ*, 218
- Liu, C., Deng, L.-C., Carlin, J. L., et al. 2014, *ApJ*, 790, 110
- Luo, A.-L., Zhang, H.-T., Zhao, Y.-H., et al. 2012, *Research in Astronomy and Astrophysics*, 12, 1243
- Luo, A.-L., Zhang, Y.-X., & Zhao, Y.-H. 2004, *Proc. SPIE*, 5496, 756
- Luo, A.-L., Zhao, Y.-H., Zhao, G., et al. 2015, *Research in Astronomy and Astrophysics*, 15, 1095
- Mann, A. W., Gaidos, E., Lépine, S., & Hilton, E. J. 2012, *ApJ*, 753, 90
- Molenda-Żakowicz, J., Frasca, A., & Latham, D. W. 2008, *Acta Astron.*, 58, 419
- Molenda-Żakowicz, J., Sousa, S. G., Frasca, A., et al. 2013, *MNRAS*, 434, 1422
- Monet, D. G., Levine, S. E., Canzian, B., et al. 2003, *AJ*, 125, 984
- Morel, T., & Miglio, A. 2012, *MNRAS*, 419, L34
- Niemczura, E., Murphy, S. J., Smalley, B., et al. 2015, *MNRAS*, 450, 2764
- Petigura, E. A., Marcy, G. W., & Howard, A. W. 2013, *ApJ*, 770, 69
- Plavchan, P., Bilinski, C., & Currie, T. 2014, *PASP*, 126, 34
- Stoughton, C., Lupton, R. H., Bernardi, M., et al. 2002, *AJ*, 123, 485
- Su, D. Q., Cui, X., Wang, Y., & Yao, Z. 1998, *Proc. SPIE*, 3352, 76
- Tkachenko, A., Lehmann, H., Smalley, B., Debosscher, J., & Aerts, C. 2012, *MNRAS*, 422, 2960

- Tkachenko, A., Lehmann, H., Smalley, B., & Uytterhoeven, K. 2013, MNRAS, 431, 3685
- Thygesen, A. O., Frandsen, S., Bruntt, H., et al. 2012, A&A, 543, A160
- Uytterhoeven, K., Briquet, M., Bruntt, H., et al. 2010a, Astronomische Nachrichten, 331, 993
- Uytterhoeven, K., Szabo, R., Southworth, J., et al. 2010b, arXiv:1003.6089
- Uytterhoeven, K., Moya A., Grigahcène A., et al. 2011, A&A, 534, A125
- Valenti, J. A., & Piskunov, N. 1996, A&AS, 118, 595
- Wang, S.-G., Su, D.-Q., Chu, Y.-Q., Cui, X., & Wang, Y.-N. 1996, Appl. Opt., 35, 5155
- Wei, P., Luo, A., Li, Y., et al. 2014, AJ, 147, 101
- Wu, Y., Luo, A.-L., Shi, J. *, et al. 2010, Progress in Astronomy, 28, 404
- Wu, Y., Du, B., Luo, A., Zhao, Y., & Yuan, H. 2014a, IAU Symposium, 306, 340
- Wu, Y., Luo, A.-L., Li, H.-N., et al. 2011a, Research in Astronomy and Astrophysics, 11, 924
- Wu, Y., Singh, H. P., Prugniel, P., Gupta, R., & Koleva, M. 2011b, A&A, 525, A71
- Xie, J. W., Dong, S. B., et al. 2016, submitted
- Zhao, G., Zhao, Y.-H., Chu, Y.-Q., Jing, Y.-P., & Deng, L.-C. 2012, Research in Astronomy and Astrophysics, 12, 723
- Zhong, J., Chen, L., Liu, C., et al. 2014, ApJ, 789, L2